LA-UR-14-27538
Approved for public release; distribution is unlimited.

Title: Chancellor Water Colloids: Characterization and Radionuclide Associated Transport

Author(s): Reimus, Paul William
Boukhalfa, Hakim

Intended for: Report

Issued: 2014-09-26

Final Report

Chancellor Water Colloids: *Characterization and Radionuclide Associated Transport*

Prepared by:

Paul W. Reimus

and

Hakim Boukhalfa

Los Alamos National Laboratory
Earth and Environmental Sciences Division (EES-14)
P.O. Box 1663, Mail Stop J966
Los Alamos, NM 87545
Ph.: (505) 665-2537, 667-7219
Fax: (505) 606-2258
E-Mail: preimus@lanl.gov, hakim@lanl.gov

Contributors

Naomi Wasserman
Bryan Erdmann
Amr I. Abdel-Fattah
S. Doug Ware
Peng He
Sowmitri Tarimala
Bennie Martinez

September, 2014

Abstract

Column transport experiments were conducted in which water from the Chancellor nuclear test cavity was tranported through crushed volcanic tuff from Pahute Mesa. In one experiment, the cavity water was spiked with solute ^{137}Cs, and in another it was spiked with $^{239/240}$Pu(IV) nanocolloids. A third column experiment was conducted with no radionuclide spike at all, although the ^{137}Cs concentrations in the water were still high enough to quantify in the column effluent. The radionuclides strongly partitioned to natural colloids present in the water, which were characterized for size distribution, mass concentration, zeta potential/surface charge, critical coagulation concentration, and qualitative mineralogy. In the spiked water experiments, the unanalyzed portion of the high-concentration column effluent samples were combined and re-injected into the respective columns as a second pulse. This procedure was repeated again for a third injection.

Measurable filtration of the colloids was observed after each initial injection of the Chancellor water into the columns, but the subsequent injections (spiked water experiments only) exhibited no apparent filtration, suggesting that the colloids that remained mobile after relatively short transport distances were more resistant to filtration than the initial population of colloids. It was also observed that while significant desorption of ^{137}Cs from the colloids occurred after the first injection in both the spiked and unspiked waters, subsequent injections of the spiked water exhibited much less ^{137}Cs desorption (much greater ^{137}Cs colloid-associated transport). This result suggests that the ^{137}Cs that remained associated with colloids during the first injection represented a fraction that was more strongly adsorbed to the mobile colloids than the initial ^{137}Cs associated with the colloids. A greater amount of the $^{239/240}$Pu desorbed from the colloids during the second column injection compared to the first injection, but then desorption decreased significantly in the third injection. This result suggests that the Pu(IV) nanocolloids probably at least partially dissolved during and after the first injection, resulting in enhanced desorption from the colloids during the second injection, but by the third injection the Pu started following the same trend that was observed for ^{137}Cs. The experiments suggest a transport scale dependence in which mobile colloids and colloid-associated radionuclides observed at downstream points along a flow path have a greater tendency to remain mobile along the flow path than colloids and radionuclides observed at upstream points. This type of scale dependence may help explain observations of colloid-facilitated Pu transport over distances of up to 2 km at Pahute Mesa.

1. Introduction

Between 1951 and 1992 over 800 underground nuclear tests were conducted at the Nevada Test Site, now called the Nevada National Security Site (NNSS). Approximately 2/3rds of these tests were conducted at or below the water table, leaving a significant inventory of radionuclides behind to potentially migrate in the groundwater. Colloid-facilitated transport is generally considered to be the most likely mechanism for transport of low-solubility, strongly adsorbing radionuclides over significant distances at the NNSS (where groundwater pHs are typically neutral to slightly basic (7-8.5) and natural organic carbon concentrations in the waters are low). Buddemeier and Hunt (1988) first reported strong colloid associations of low-solubility refractory radionuclides in NNSS groundwaters. Kersting et al. (1999) reported colloid-associated Pu transport over a distance of 1.3 km in ~30 years from the Benham nuclear test cavity on Pahute Mesa at the NNSS. It has since been confirmed that Pu from the Benham

cavity has migrated an additional 0.8 km downgradient (Zavarin, 2012) after ~45 years. Kersting and Zavarin (2011) and Kersting (2013) summarize many other observations of colloid-facilitated radionuclide transport over significant distances at various locations around the world.

Although the concentrations of Pu and other radionuclides associated with colloids in NNSS ground waters have never been measured high enough to be considered a risk to human health (even at nuclear test cavity source locations), the transport of strongly-adsorbing radionuclides such as Pu over km distance scales is an observation that attracts attention and raises questions about how well the processes responsible for the observed behavior are understood and how well the behavior can be predicted. Reimus (2003), in Kersting and Reimus (2003), concluded that the key requirements for colloid-facilitated radionuclide transport over long time and distance scales are:

(1) the radionuclide desorption rate from the colloids must be slow enough that a fraction of the mass sorbed to the colloids at the source remains sorbed to the colloids during the time it takes to move the distance in question, and
(2) the irreversible filtration rate of the colloids must be slow enough that a fraction of the colloids at the source is not filtered during the time it takes to move the distance in question.

If these kinetic limitations aren't met, then colloid concentrations must be extremely high and equilibrium radionuclide partitioning to colloids must be much stronger than to competing immobile surfaces to have any possibility of colloid-facilitated transport over significant distances. These conditions are unlikely to exist except under very extreme circumstances.

Kersting and Zavarin (2011) and Kersting (2013) provide good summaries of recent work that has advanced the understanding of colloid-facilitated radionuclide transport processes, particularly from the standpoint of characterizing radionuclide-colloid associations. However, the ability to predict colloid-facilitated transport over the long time and distance scales of relevance for environmental risk assessments has remained elusive.

In this report, we describe an experimental investigation aimed at addressing, to the extent possible in relatively short-duration laboratory experiments, the two key kinetic requirements listed above for colloid facilitated radionuclide transport over significant time and distance scales. Although colloid characterization results and radionuclide-colloid association measurements are presented in the report, the key findings are derived from a series of column transport experiments in which colloids and radionuclides that had already transported through a column once were re-injected into the same column a second time and then a third time. This procedure was employed to evaluate whether the colloids that had transported through the column were more likely to transport through a second and third time, and likewise whether colloid-associated radionuclides that transported through the columns were more likely to remain associated with the colloids when transported through again.

We chose to focus on colloids from the Chancellor nuclear test cavity at the NNSS because this cavity water has unusually high concentrations of ^{137}Cs and $^{239/240}$Pu compared to other NNSS cavity waters, and both of these radionuclides were already known to be quite strongly associated with colloids in the water (Reimus et al., 2006; Rose et al, 2011). The high radionuclide concentrations in the Chancellor cavity water may be related to a hydrologic isolation of the cavity that is also inferred from high residual temperatures and more reducing

redox conditions than is typical of cavity waters at the NNSS (Rose et al., 2011). While we recognize that such hydrologic conditions would tend to limit colloid and radionuclide transport out of the cavity, thus reducing the potential relevance of experimental results obtained using Chancellor water, there appears to be nothing unique about the properties of Chancellor water colloids relative to other NNSS cavity waters, and it is quite possible that similar radionuclide concentrations and temperatures existed in more hydrologically-connected cavities at early times after nuclear detonation.

2. Materials and Methods

2.1 Chancellor Cavity Water

Two 55-gallon drums of water were collected from borehole U-19adPS#1a soon after it was drilled into the Chancellor nuclear test cavity in 2004. Chancellor water was used for this study because it has relatively high colloid concentrations and very high $^{239/240}$Pu concentrations compared to other NNSS cavity waters, and most of the Pu is associated with the colloids (Reimus et al., 2006, Appendix C; Rose et al., 2011). It is the only cavity water we are aware of in which the alpha activity is dominated by $^{239/240}$Pu rather than by uranium isotopes. The major ion chemistry of the water, as reported in the UGTA geochemistry database for a sample collected from U-19adPS#1a on 5/1/08, is reflected in the synthetic water recipe of Table 1. This recipe was used to prepare water that served as colloid-free and radionuclide-free background water in the column transport experiments described below. The silica concentration of the synthetic water was reduced relative to that measured in Chancellor water because the Chancellor water was 65-75^{o}C when it was collected, and the experiments of this study were conducted at room temperature (20-25^{o}C) where the silica solubility limit would be much lower. We wanted to avoid precipitation of silica, which would produce silica colloids that might affect the experiment results. The synthetic water pH was also slightly lower than that reported in the

Table 1. Synthetic Chancellor water recipe and major constituent concentrations.

Recipe based on Salts

Salt	Conc. (mg/L)
$CaCl_2$	3.105
KCl	8.895
$MgCl_2$	1.802
NaCl	31.90
Na_2SO_4	93.72
$NaHCO_3$	135.150
Na_2CO_3	37.165
H_4SiO_4	40.00
pH[1]	8.7
Ionic Strength	0.0054 M

Major Constituent Concentrations, mg/L

Constituent	Recipe	UGTA Database[2]
Na^+	96.0	96
K^+	4.67	4.66
Ca^{++}	1.12	1.12
Mg^{++}	0.46	0.46
Cl^-	26.9	26.9
$SO_4^=$	63.4	63.4
$HCO_3^-/CO_3^=$	119.2	119-126
SiO_2	25.0	115.3[3]
pH	8.7	8.9

[1] Adjusted using NaOH or HCl

[2] Values are for sample collected 5/1/2008, except for $HCO_3^-/CO_3^=$, which is from 9/27/2004 sample ($HCO_3^-/CO_3^=$ was not reported in 2008).

[3] SiO_2 value was taken from Rose et al. (2011) – not reported in UGTA database.

UGTA geochemistry database because we wanted it to match the pH of the Chancellor water in our lab at the atmospheric conditions in Los Alamos.

2.2 Water Extraction from Drums and Filtration Procedure

Without any stirring or agitation, water from near top of one of the 55-gallon drums was pumped into a 2-gallon Nalgene jug using a peristaltic pump. The tubing and container were pre-cleaned before the operation. About 1.5 liters of the extracted sample were filtered through a 100,000 NMWL filtration membrane followed by an inline 0.02 μm syringe filter. The filtration was carried out in an filtration cell (350 ml) operated under pressure (~15-20 psi). The same membrane was retained for the entire filtration process but the 0.02 μm syringe filter was changed every ~500 ml. The above collection and filtration procedure was repeated after the contents of the 55-gallon drum were stirred vigorously with a long nylon rod to scrape the bottom and stir up and re-suspend settled or deposited colloids. Water was extracted using a peristaltic pump 2 hours after the sample was stirred which allowed any large, non-colloidal particles to settle. The stirred and unstirred samples, both filtered and unfiltered, were analyzed for radionuclide content by liquid scintillation counting and for colloid characteristics as described below.

2.3 Water Centrifugation Procedure

In addition to ultrafiltration, colloids were also separated from the Chancellor water by centrifugation. This procedure involved spinning unfiltered water samples at 55,000 rpm in a high-speed centrifuge (resulting in about 170,000 g) for at least 1.5 hours, after which the supernatant could be separated from the solids by decanting or pipetting out of the centrifuge tube. Assuming spherical colloids with 2.6 g/cm^3 density, this centrifugation procedure should have effectively removed colloids greater than about 10 nm diameter from the supernatant.

2.4 Colloid Size Distribution and Concentration Measurements

Colloid size distribution and concentration analyses were performed using a laser particle spectrometer (Particle Measuring Systems, Inc.). The spectrometer simultaneously counts and sizes individual colloids in a highly focused and diluted aqueous sample stream that is passed through a laser beam. Size bins range from 50 to 1000 nm and are based on the amount of light scattered by the colloids. 8 ml of unfiltered water was collected from both the stirred and unstirred drums in clean plastic centrifuge tubes for analysis. Also, two 8 ml samples of ultra-filtered water (stirred and unstirred) were collected after filtration through both the 100,000 NMWL membrane filter and the 0.02 μm syringe filter. All samples were diluted 200 times prior to analysis (in addition to the dilution internal to the laser spectrometer) to avoid count rates that would saturate the detector. Deionized water was used for dilution, which was also analyzed to account for background colloids.

The mass concentration of colloids in the Chancellor water was estimated by weighing the solids obtained after centrifuging a known volume of the water (500 mL) and evaporating the separated solids to dryness. A correction was made for total dissolved solids in the water by subtracting the weight of solids remaining after evaporating a known volume of supernatant from centrifugation.

2.5 Surface Charge Measurements (Zeta (ζ) Potential)

Colloid surface charge measurements were performed on 2 mL aliquots of different samples using a Malvern Zetasizer. The zeta potential (mV) of the colloids, or the potential at the plane of hydrodynamic shear when the colloids are induced to move in an electric field, was used as a measure of the surface charge. Each measurement consisted of an average of 5 runs spaced 1 minute apart. Another longer duration measurement was carried out on each of the samples with 100 runs spaced 1 minute apart.

2.6 Colloid Stability and Critical Coagulation Concentration (CCC)

The coagulation kinetics of the Chancellor water colloids was measured at different ionic strengths and pH values using the Malvern Zetasizer instrument. The early-stage coagulation rate (doublet formation rate) was determined as the slope of the Z-average size versus time plot in the first few minutes. The Z-average size is the intensity-weighted mean hydrodynamic size of the ensemble collection of colloids measured by dynamic light scattering (Malvern Zetasizer Technical Note MRK-1515-01). The critical coagulation concentration was taken to be the ionic strength above which the early-stage coagulation rate no longer increased.

2.7 Colloid Mineralogy

X-ray diffraction (XRD) analysis was conducted on a sample of the Chancellor water colloids. The colloids were collected from the water using the centrifugation procedure described above (170,000 g for 90 min.). The collected sample was dried and weighed to determine its exact mass and mixed with 20 wt.% of corundum (Al_2O_3). The sample plus corundum was ground and homogenized before analysis. The powdered sample was deposited on a low-background quartz plate coated with a thin layer of silicon vacuum grease to prevent dispersion of the powder. The sample mount is shown in Figure 1. The X-ray diffraction (XRD) analysis was performed with a Bruker D8 diffractometer using Cu-Kα radiation. Data were collected from 7 to 80° 2θ with a 0.02º 2θ step-size and count times of 16 seconds per step.

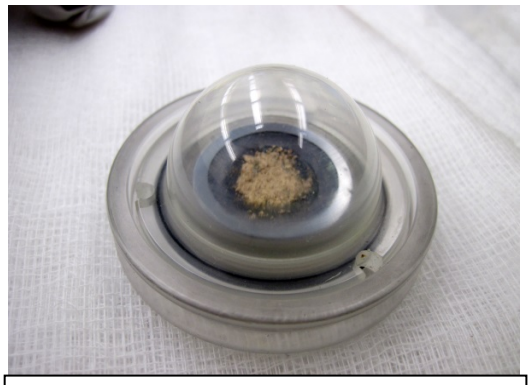

Figure 1. Sample mount used for XRD analysis of the colloids.

Colloid samples were also deposited onto pin mounts for SEM/EDS analysis, but these analyses were never completed because the instrument that was to be used for these radiological samples was overcommitted to a national security program.

2.8 Tuff used in Column Transport Experiments

The material used in the column transport experiments was crushed tuff from NNSS borehole UE-20c, 2751-2755 ft below surface, identified by Drellack and Prothro (1997) as being moderately-welded Topapah Spring Tuff, Pahute Mesa lobe. UE-20c is within 2 km of the ER-20-5 wells where colloid-facilitated Pu transport originating from the Benham nuclear test cavity was first observed (Kersting et al., 1999), and the core was taken from the same unit that ER-20-5 #1 is completed in (ER-20-5 #1 had the highest concentrations of Pu from the Benham cavity). Prior to packing, the crushed tuff was wet-sieved to a size range of 125 to 2000 µm, which resulted in column porosities of approximately 50%. A more detailed description of

the tuff, including information on its mineralogy and other characteristics, is providing in Appendix A (taken from Reimus et al., 2002).

The use of crushed tuff to represent what is actually a fractured rock aquifer was not considered ideal, but it was the only way we could devise a laboratory flow system with enough pore volume to get good breakthrough curve resolution and still have plenty of eluted volume left over for repeat injections. We expect that the use of crushed tuff should have resulted in greater colloid filtration and radionuclide desorption from colloids than in a fracture flow system (for a given transport distance and residence time) because the surface area to volume ratio in a crushed rock system should be larger than in a fracture flow system. However, the fracture coating mineralogy may not have been well represented by the crushed tuff.

2.9 Radionuclide Concentrations by Liquid Scintillation Counting (LSC)

For analyzing radionuclide concentrations, 5 ml aliquots of filtered and unfiltered samples from the stirred and unstirred drum were pipetted into plastic liquid scintillation vials, and then 15 mL of Ultima Gold AB scintillation cocktail was added to each vial to bring the total volume to 20 mL. For samples from the column experiment (below), 6-mL aliquots were combined with 14 mL of Ultima Gold AB cocktail. The samples were shaken vigorously before transferring to either a Perkin-Elmer Tri-Carb Model 2500 or a Perkin-Elmer Quantulus scintillation counter, where they were counted for 6 to 10 hours. The Quantulus scintillation counter is designed for ultra-low level combined beta and alpha decay counting of environmental samples.

2.10 Radionuclide-Colloid Association Measurements.

Radionuclide associations with the Chancellor colloids were determined after either filtration or centrifugation (procedures described above). In the case of the filtered samples, the filtrate was assumed to contain only the solute portion of the radionuclide mass, and the difference between the unfiltered and filtered samples was taken to be the colloid-associated mass fraction. A similar procedure was followed for the centrifuged samples; the supernatant was assumed to contain the solute portion of radionuclide mass, and the difference between the uncentrifuged and centrifuged sample was taken to be the colloid-associated mass fraction.

It was ultimately determined that ^{137}Cs was the only radionuclide besides ^{3}HHO that could be quantified in the Chancellor water by inexpensive liquid scintillation counting (above). The $^{239/240}$Pu activity, while very high for a NNSS cavity water, was still nearly 3 orders of magnitude lower than the ^{137}Cs activity, which made it impossible to use liquid scintillation counting for $^{239/240}$Pu measurements. Thus, for the Pu column experiments $^{239/240}$Pu was spiked into the Chancellor water to allow the use of liquid scintillation counting, and the partitioning of the Pu between the solute and colloid phases was determined as described above. The spiked Pu was introduced as Pu(IV) nanocolloids or 'intrinsic colloids', with all dissolved-phase Pu removed or at least minimized by centrifugation (see next section).

2.11 Preparation of Pu(IV) Intrinsic Colloids

Plutonium colloid suspensions were prepared following a modified sol-gel procedure in which polymerization of a nitric acid solution containing pure Pu(IV) was attained by slowly increasing the pH using NH_4OH (25%) (Abdel-Fattah et al., 2013). The Pu(IV) precipitate was washed

carefully and re-suspended in distilled nanopure water, and the pH was adjusted to 4.26 and left to age for about two years. The Pu was verified spectroscopically to still consist almost entirely of Pu(IV) intrinsic colloids after two years. The properties of the intrinsic colloids are described in detail by Abdel-Fattah et al. (2013).

The plutonium colloids used in the column experiments were prepared from the aged Pu(IV) stock solution after washing repeatedly with deionized water and centrifuging at 170,000 g for 90 min. to remove any soluble plutonium (repeated until the supernatant registered very low activity). The resuspended intrinsic colloids were sonicated to disperse large aggregates and filtered using a 0.22-μm polycarbonate filter to remove any remaining aggregates but allow the small intrinsic colloids to pass. The filtered sample was allowed to settle overnight in the dark before sampling. An aliquot was removed from the solution and was diluted in the Chancellor water to obtain the desired Pu concentration. Although we did not measure the size distribution of the Pu(IV) colloids used in our experiments, we know they were much smaller than the majority of the natural Chancellor colloids because of both their preparation procedure (the 0.22-μm filter removed the vast majority of the natural colloids) and the fact that the natural colloids could be centrifuged out of suspension much more readily than the Pu(IV) colloids (see Section 3.4.3). The differential centrifugation properties of the two different types of colloids were exploited to determine the fraction of Pu(IV) colloids associated with the natural colloids.

2.12 Column Transport Experiments

Two 60-cm long by 2.6-cm diameter glass columns were used for the column transport experiments. The columns were thoroughly washed and rinsed with de-ionized water prior to packing. The packing material in both columns was the crushed tuff described in Section 2.8. The columns were saturated using synthetic ground water prepared according to the recipe of Table 1. To avoid air bubbles that might trap colloids, the columns were saturated by first evacuating them under house vacuum, then filling with CO_2 gas, and then evacuating again before introducing degassed water under vacuum. The two columns were aligned vertically with flow from bottom to top (Figure 2). Syringe pumps (KD Scientific) were used to maintain a controlled flow rate with minimal pulsing. A linear flow velocity of about 30 cm/day (110 m/year) was established as the target velocity. Column effluent was collected in either plastic test tubes or Falcon centrifuge tubes, and these samples were transferred to Teflon test tubes soon after collection.

Figure 2. Photo of columns used for the column transport experiments.

The ^{3}HHO that was naturally present in the Chancellor water was used as a conservative solute tracer in all the column experiments. It could be readily distinguished from the ^{137}Cs and $^{239/240}$Pu by liquid scintillation counting because of its very high abundance and much lower decay energies relative to these nuclides. The transport parameters for the colloids and radionuclides could then be deduced by fitting their breakthrough curves as well as the ^{3}HHO breakthrough curve using an appropriate transport model (Section 2.13).

2.12.1 Chancellor Water Experiment

The first experiment was conducted in one of the columns using unfiltered Chancellor water. The columns were initially flushed with the synthetic Chancellor water at a flow rate of ~4.0 mL/hr using two syringe pump set at 2.0 mL/hr each. Flushing continued until the concentration of colloids in the effluent samples dropped to a background in the range of 3×10^{8}/ml, or about two orders of magnitude lower than the concentration in the Chancellor water. The concentrations of background colloids were measured using the laser particle spectrometer (Particle Measurement Systems, Inc.).

An injection sample was obtained from a fully homogenized (stirred) Chancellor water drum. The sample was sonicated for 30 sec. and degassed by stirring vigorously under house vacuum prior to loading into the injection syringes. A sample was collected from the syringe prior to the start of the injection and counted to determine the colloid and ^{137}Cs concentration. The colloid concentration was approximately 2.68 x 10^{10} colloids/ml and the ^{137}Cs concentration was about 34 dpm/ml, or about 1.56 x 10^{4} pCi/L (see Table 2). A total of 252 ml was injected using 5 separate syringes of about 50 mL each. The column injection rate was set to 4.0 ml/hr, and effluent samples were collected every 2.5 hrs using an automatic fraction collector. The effluent samples were analyzed for tritium and ^{137}Cs activity by liquid scintillation counting (Quantulus scintillation counter), as described above. Several of the effluent samples were also analyzed for colloid concentrations using the laser particle spectrometer system. The highest concentration effluent samples were diluted 200 times to get an accurate count rate on the laser spectrometer. The Chancellor water was also diluted 200 times to get an accurate colloid count rate.

2.12.2 Spiked Chancellor Water Experiments with Multiple Injections

The Chancellor water experiment was followed by two separate experiments involving unfiltered Chancellor water that was spiked with Cs and $^{239/240}$Pu, respectively. The experiments were conducted in the two respective columns, with the Pu being injected in the same column that was used for the unspiked Chancellor water experiment. This column was kept flowing at a very low flow rate between the two experiments (about six months). A unique aspect of the experiments was that a significant fraction of the colloids and radionuclides recovered after one injection were re-injected into the same column. This procedure was repeated twice for a total of three injections in each column.

2.12.2.1 ^{137}Cs Experiments

The Cs-spiked Chancellor water solution was prepared by adding 1.5 ml of a stock solution containing 0.15 mM CsCl spiked with a small amount of ^{137}Cs to 1 L of natural unfiltered Chancellor water. The solution was shaken continually for 1 week prior to its use in the column transport experiments. The total activity from ^{137}Cs in the injection solution was determined to be 1.84 x 10^{4} pCi/L, which was about 18% higher than the 1.56 x 10^{4} pCi/L in the unspiked

water (Table 2). However, the spike increased the overall concentration of Cs in the Chancellor water by about 5 orders of magnitude. The rationale for this spike was to see if the significant increase in the overall Cs concentration would cause a shift in the partitioning of ^{137}Cs between the colloids and the solution phase. If the spike caused a significant shift, then it could be concluded that the colloid surfaces had reached capacity with respect to the amount of ^{137}Cs that could be adsorbed to them (after the spike). If the spike did not cause a shift in ^{137}Cs partitioning, then it could be concluded that either the colloid surfaces had not reached sorption capacity or the ^{137}Cs originally adsorbed to the colloids was not readily exchanging with the spiked Cs.

Table 2 lists the colloid and ^{137}Cs concentrations in the first injection solution and in the two subsequent injection solutions. The volumes of each injection are also listed. The injection volumes decreased with each successive injection because a significant fraction of the water that eluted from the columns was expended for analyses of the colloids and radionuclides. The remaining unanalyzed samples or fractions of samples from the portion of each injection experiment that had relatively high colloid and ^{137}Cs concentrations were combined into a single solution and used for the next injection. An aliquot of this solution was analyzed for ^{137}Cs partitioning to the colloids, as well as for overall colloid and ^{137}Cs concentrations.

The colloid concentration in the first Cs-spiked injection solution was significantly lower (nearly 22% lower) than in the unspiked Chancellor water experiment. We do not have an explanation for this discrepancy other than that perhaps there was an inconsistency in the way the 55-gallon drums were sampled for the different experiments. However, it is noteworthy that Reimus et al. (2006) reported a colloid concentration in the unfiltered Chancellor water of about 3.9×10^{10} colloids/ml, which is about 40% higher than in the unspiked water experiment and nearly twice that measured for the first Cs-spiked injection solution. These results suggest there may have been a gradual lowering of colloid concentrations in the 55-gallon drums over time due to either slow aggregation and/or settling of the colloids (not reversible by stirring), or perhaps due to colloid attachment to the plastic drum walls. Whatever their cause, we do not believe that these apparent decreases in colloid concentrations affected the results of the transport experiments because (1) the ^{137}Cs association with colloids in the Chancellor water was nearly the same at all the different times measured regardless of the apparent colloid concentrations, and (2) the colloid concentrations in the column experiments were always normalized to the colloid injection concentration. The colloid concentrations in the second and third injections were somewhat lower than in the first injection (Table 2) but not significantly different from each other, suggesting some colloid filtration after the first injection, but not after the second injection.

Table 2. Injection volumes, colloid concentrations, and Cs concentrations in the three successive column injections of Cs-spiked Chancellor water. The corresponding values for the unspiked Chancellor water experiment are provided for comparison.

Injection	Volume Injected, ml	Colloid Conc., colloids/ml	Cs Conc., M	^{137}Cs Activity, pCi/L
1	662	2.08×10^{10}	2.24×10^{-7}	1.84×10^{4}
2	200	1.85×10^{10}	2.67×10^{-8}	2.19×10^{3}
3	140	1.85×10^{10}	1.46×10^{-8}	1.20×10^{3}
Unspiked	252	2.68×10^{10}	1.3×10^{-12}	1.56×10^{4}

The first and third Cs-spiked injections were conducted with combined syringe pump settings of 4 ml/hr, although the calculated flow rates were closer to 3.8 ml/hr. For the second injection, one of the two syringe pumps failed very soon after the injection was started, so the flow rate for this injection was about half that for the other injections.

2.12.2.2 $^{239/240}$Pu Experiments

The $^{239/240}$Pu-spiked Chancellor water solution was prepared to make it possible to quantify Pu concentrations in the column experiments by inexpensive liquid scintillation counting. The spiked solution was prepared by adding 0.20 ml from a stock solution of intrinsic Pu(IV) colloids (see Section 2.11 for preparation details) to 10.0 ml of natural Chancellor water from which most of the colloids had been removed by centrifuging at 16,000 RPM for 10 min. The spiked 10 ml solution was sonicated for 10 min and then filtered through a 0.22 um polycarbonate filter. 9.8 ml of the filtrate was added to a Teflon bottle containing 990 ml of natural Chancellor water. This solution was sonicated for 30 sec. and left on a mechanical shaker to equilibrate for a week before its injection into the column. The final plutonium concentration in the Chancellor water used for the first injection was estimated to be 0.63 ng/L, based on liquid scintillation counting.

Table 3 lists the injection volumes and the natural colloid and $^{239/240}$Pu concentrations in each of the three injections for the $^{239/240}$Pu-spiked Chancellor water experiments. As in the Cs-spiked experiment(s), the remaining unanalyzed samples or fractions of samples from the portion of each injection experiment that had relatively high colloid and $^{239/240}$Pu concentrations were combined into a single solution and used for the next injection. Also, an aliquot of this solution was analyzed for $^{239/240}$Pu partitioning to the colloids, as well as for the overall colloid and $^{239/240}$Pu concentrations. The colloid concentration in the first injection solution listed in Table 3 is in reasonable agreement with that for the first Cs-spiked injection (Table 2), suggesting good consistency between the preparations of the solutions for the two sets of experiments. As in the case of the Cs-spiked experiments, the colloid concentrations in the second and third injections were lower than in the first injection but not significantly different from each other, suggesting colloid filtration in the column after the first injection, but not after the second injection.

The flow rate for all the Pu-spiked injections was about 3.6 ml/hr (two syringe pumps with combined settings of 4 ml/hr).

Table 3. Injection volumes, colloid concentrations, and $^{239/240}$Pu concentrations in the three successive column injections of Pu-spiked Chancellor water.

Injection	Volume Injected, ml	Colloid Conc., colloids/ml	Pu Conc., M	$^{239/240}$Pu Activity, pCi/L
1	704	1.80×10^{10}	2.64×10^{-9}	3.91×10^{4}
2	377	1.22×10^{10}	2.26×10^{-9}	3.34×10^{4}
3	190	1.29×10^{10}	1.26×10^{-9}	1.86×10^{4}

2.13 Modeling of Column Transport Experiments

The conceptual model initially conceived to match the column transport data was a 1-D advection-dispersion model that accounted for conservative transport of ^{3}HHO, colloid filtration and detachment, and either Cs or Pu adsorption and desorption to/from the crushed tuff used to

pack the column and also sorption and desorption to/from the colloids (both mobile and immobile). The equations accounting for all these processes are:

Mobile ^{3}HHO:
$$\frac{\partial C_H}{\partial t} + v_s \frac{\partial C_H}{\partial x} - D_s \frac{\partial^2 C_H}{\partial x^2} = 0 \quad (1)$$

Mobile Colloids:
$$\frac{\partial C_{col}}{\partial t} + V_c \frac{\partial C_{col}}{\partial x} - D_c \frac{\partial^2 C_{col}}{\partial x^2} + k_{fc} C_{col} - k_{rc} S_{col} = 0 \quad (2)$$

Immobile Colloids:
$$\frac{\partial S_{col}}{\partial t} - k_{fc} C_{col} + k_{rc} S_{col} = 0 \quad (3)$$

Mobile Solute Cs or Pu (or intrinsic Pu Colloids):
$$\frac{\partial C}{\partial t} + v_s \frac{\partial C}{\partial x} - D_s \frac{\partial^2 C}{\partial x^2} + \left(\frac{\rho_B}{\phi}\right) k_{fs} C + k_{fsc} C C_{col} + k_{fsc} C S_{col} - \left(\frac{\rho_B}{\phi}\right) k_{rs} S - k_{rsc} C_1 - k_{rsc} C_2 = 0 \quad (4)$$

Cs or Pu Immobilized on Crushed Tuff:
$$\frac{\partial S}{\partial t} - k_{fs} C + k_{rs} S = 0 \quad (5)$$

Cs or Pu Adsorbed to Mobile Colloids:
$$\frac{\partial C_1}{\partial t} + v_c \frac{\partial C_1}{\partial x} - D_c \frac{\partial^2 C_1}{\partial x^2} - k_{fsc} C C_{col} - k_{rc} C_2 + k_{fc} C_1 + k_{rsc} C_1 = 0 \quad (6)$$

Cs or Pu Adsorbed to Immobile Colloids:
$$\frac{\partial C_2}{\partial t} - k_{fsc} C S_{col} - k_{fc} C_1 + k_{rc} C_2 + k_{rsc} C_2 = 0 \quad (7)$$

where, C_{col} = concentration of colloids in mobile solution phase, g/cm^3
S_{col} = colloid concentration on tuff surfaces, g/cm^3
C = concentration of Cs or Pu or in solution, g/cm^3
C_H = concentration of ^{3}HHO in solution, g/cm^3
S = concentration of Cs or Pu sorbed to tuff surfaces, g/g
C_1 = concentration of Cs or Pu sorbed to mobile colloids, g/cm^3
C_2 = concentration of Cs or Pu sorbed to immobile colloids, g/cm^3
V_s = solute fluid velocity, cm/s
V_c = colloid fluid velocity, cm/s
D_s= solute dispersion coefficient, cm^2/s
D_c = colloid dispersion coefficient, cm^2/s
ρ_B = bulk density of tuff, g/cm^3
ϕ = column porosity
k_{fc} = colloid filtration rate constant (1/s) = λv_f, where λ = filtration coefficient (1/cm)
k_{rc} = colloid detachment rate constant, 1/s.

k_{fs} = rate constant for sorption of Cs or Pu onto tuff surfaces, ml/g-s
k_{rs} = rate constant for desorption of Cs or Pu from tuff surfaces, 1/s
k_{fsc} = rate constant for sorption of Cs or Pu onto colloid surface, ml/g-s
k_{rsc} = rate constant for desorption of Cs or Pu from colloid surface, 1/s
t = time, s
x = distance along column, cm.

As attempts were made to match the data, it quickly became clear that equations (2)-(7) could be simplified considerably by dropping terms or entire equations that had no apparent influence on the fits to the data. For instance, it became apparent that it was unnecessary to account for any solution phase transport of Cs or Pu (or Pu transport as Pu(IV) nanocolloids) through the columns to match the data. That is, the k_{fs} could be set to a large value, and effectively the transport equation for solute Cs or Pu (or Pu(IV) nanocolloids) (equation 4) could be eliminated in favor of simply assuming that the fraction of radionuclide mass that was not adsorbed to the Chancellor colloids at the time of injection into the columns or that desorbed from the colloids within the columns very quickly became irreversibly adsorbed to the crushed tuff in the columns. Furthermore, it was also found to be unnecessary to account for any colloid detachment from the tuff surfaces once the colloids were filtered (i.e., the colloids exhibited no tailing that would suggest detachment). These observations and assumptions allow equations (2)-(7) to be simplified to just 2 independent equations:

Mobile Colloids: $$\frac{\partial C_{col}}{\partial t} + V_c \frac{\partial C_{col}}{\partial x} - D_c \frac{\partial^2 C_{col}}{\partial x^2} + k_{fc} C_{col} = 0 \qquad (2a)$$

Cs or Pu Adsorbed to Mobile Colloids:
$$\frac{\partial C_1}{\partial t} + V_c \frac{\partial C_1}{\partial x} - D_c \frac{\partial^2 C_1}{\partial x^2} + k_{fc} C_1 + k_{rsc} C_1 = 0 \qquad (6a)$$

Equation (2a) describes colloid transport without accounting for filtered colloid concentrations because colloid filtration is assumed to be irreversible. Likewise, equation (6a) describes colloid-facilitated Cs or Pu transport without accounting for mass adorbed to immobile surfaces because once the Cs or Pu desorbs from colloids (whether mobile or immobile) or once it is immobilized by being filtered while adsorbed to colloids, this radionuclide mass is considered irreversibly lost from the system.

Equations (1), (2a) and (6a) were fitted to the column breakthrough curves in stepwise fashion using the RELAP semi-analytical model (Reimus and Haga, 1999; Reimus et al. 2003). The ^{3}HHO breakthrough curve was first fitted by adjusting the solute mean residence time (L/V_s, where L is the column length) and Peclet number (LV_s/D_s) to match the data. The colloid breakthrough curve was then fitted by adjusting the colloid mean residence time and Peclet number (L/V_c and LV_c/D_c), as well as a colloid filtration rate constant, k_{fc}, to match the data. Note that the colloids were not assumed to have the same mean residence time or Peclet number as the ^{3}HHO because of the known tendency for colloids to experience size-exclusion effects and exhibit different hydrodynamic dispersion than solutes in porous media. Finally, the colloid-associated Cs or Pu was assumed to transport according to the same parameters as the colloids,

with the only adjustable parameter being the desorption rate of the Cs or Pu from the colloids, k_{rsc}.

3. Results

3.1 Colloid Concentrations and Size Distributions in Chancellor Water

Figure 3 shows the measured colloid size distributions in 6 Chancellor water samples collected from the 55-gallon drums. Five of these samples were collected and processed at around the time of the unspiked water column experiment, with four of them measured at exactly the same time (in rapid succession on the in-situ laser spectrometer). These latter four samples were (1) unstirred unfiltered, (2) stirred unfiltered, (3) unstirred filtered, and (4) stirred filtered. The fifth sample was an aliquot of the unfiltered Chancellor water injection solution (taken directly from the 55-gallon drum) used in the unspiked water column experiment, and the sixth sample was an unfiltered sample from the same 55-gallon drum measured in 2005 (Reimus et al., 2006).

Of the four samples processed and analyzed at the same time, it is apparent from Figure 3 that stirring did not notably change the colloid concentrations and size distributions in either the filtered or unfiltered samples, although there is a big difference between filtering and not filtering. The total concentrations in the unfiltered samples over the size range from 50 to 1000 nm diameter were 1.26×10^{10}/ml (unstirred) and 1.10×10^{10}/ml (stirred). Filtration reduced the concentrations down to 6.63×10^{8}/ml and 5.97×10^{8}/ml for the unstirred and stirred samples, respectively. Thus, the filtration procedure decreased the colloid concentrations by about a factor of 19. The insignificant difference between the stirred and unstirred samples suggests that the stirring did little to re-suspend or re-disperse the colloids in the drums. The unfiltered concentrations are significantly lower than those measured in the first injection solutions for the column transport experiments (Tables 2 and 3), which may reflect the fact that the column injection solutions were sonicated but the solutions analyzed for size distributions were not sonicated. The unfiltered concentrations are over a factor of 3 lower than the 3.9×10^{10} colloids/ml reported by Reimus et al. (2006), which may reflect some aggregation or settling in the 55-gallon drums over the several intervening years, or perhaps some colloid attachment to the drum walls. It is apparent that there are significantly more colloids at the lower end of the size range in the 2005 sample and also in the sonicated injection solution than in the other two unfiltered samples.

Figure 4 shows that the vast majority of the reduction in colloid concentrations in the filtered samples relative to the unfiltered samples occurred in the size range from 50 to 100 nm diameter. The fact that there is little difference between the filtered and unfiltered concentrations beyond a size of about 150 nm diameter suggests that there are relatively few colloids in the unfiltered water greater than 150 nm in diameter (only about a factor of 2 or so more than the concentrations measured in the filtered samples).

The mass concentration of colloids in an aliquot of the stirred unfiltered sample, which yielded a colloid number concentration of 1.10×10^{10}/ml, was 0.12 g/L, or 120 mg/L. This concentration was determined using the drying and weighing method described at the end of Section 2.4. Colloid mass concentrations in other NNSS waters have not been reported to our knowledge, but based on the number concentrations reported by Reimus et al. (2006), Chancellor water appears

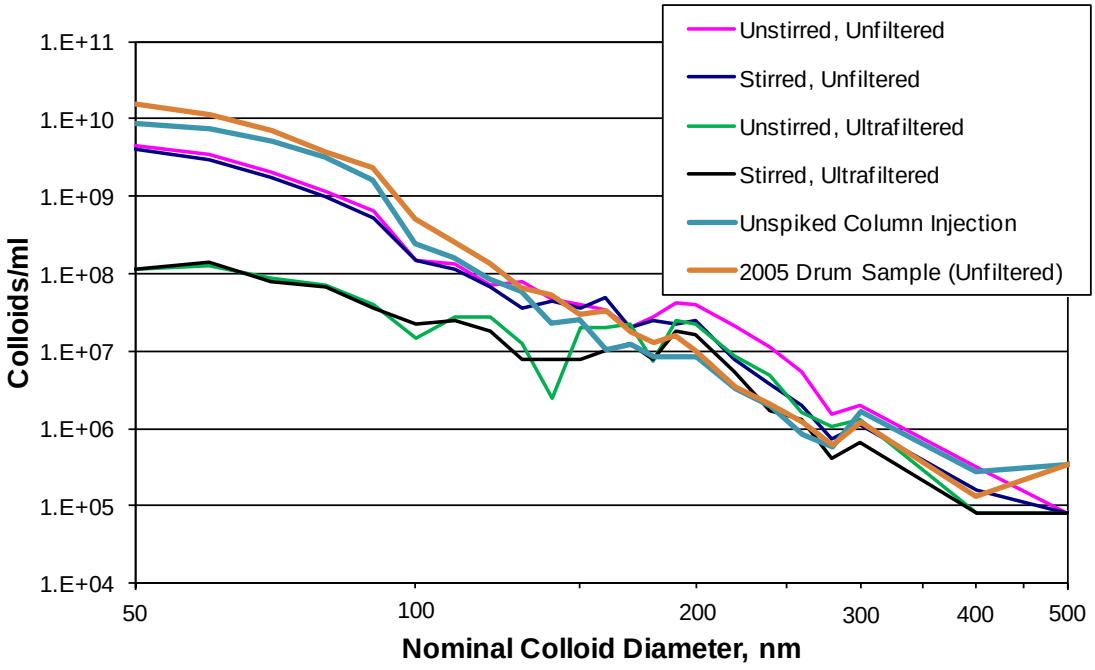

Figure 3. Colloid size distributions by in-situ laser particle spectrometer for Chancellor water samples (unspiked) collected/processed in different ways and at different times.

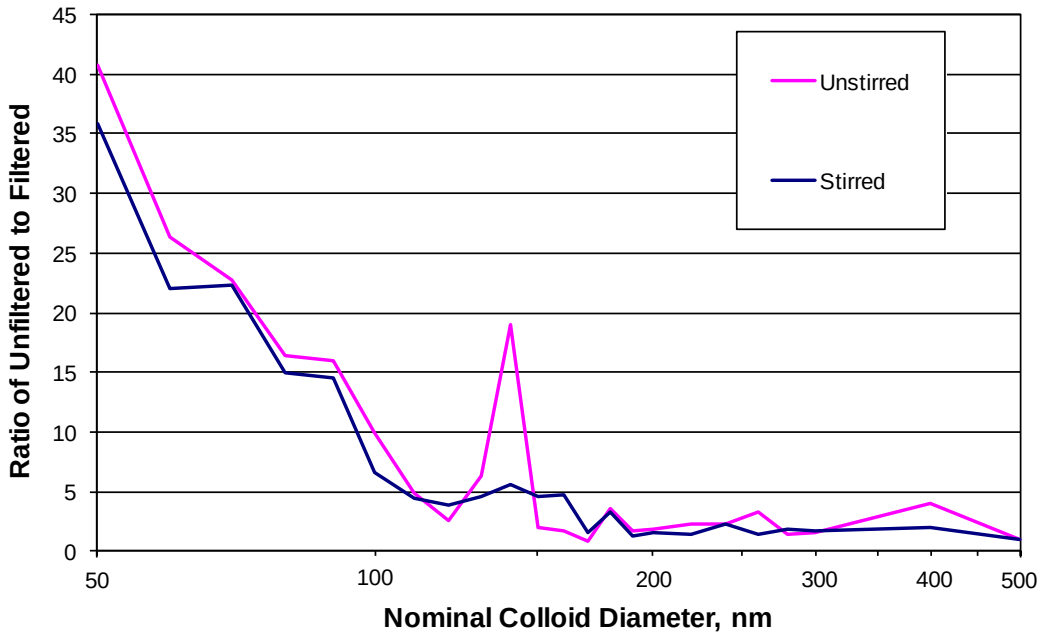

Figure 4. Ratio of unfiltered to filtered colloid concentrations as a function of colloid diameter for Chancellor water samples collected from unstirred and stirred 55-gallon drums.

to have a factor of 2-8 higher colloid concentrations than the much-studied Cheshire cavity water (U-20n), slightly lower concentrations than waters from ER-20-5#1 and ER-20-5#3, where Benham Pu was detected, over an order of magnitude lower concentrations than U4u (Dalhart

cavity), about a factor of 2-5 higher concentrations than U-3cn PS#2 (Bilby), and over an order of magnitude higher concentrations than UE-2ce (Nash) and RNM-1 (Cambric).

3.2 Colloid Zeta Potential and Stability Measurements

Measurements of the zeta potential of Chancellor colloids and of the dependence of Chancellor colloid stability on both pH and ionic strength indicated the following:

a) The zeta potential of the colloids in stirred, unfiltered samples of Chancellor water (same preparation used for the column experiments) was in the -35 to -40 mV range. These values are consistent with what is expected for silicate/clay colloids in low ionic strength ground water at a pH of ~8-9. Zeta potential measurements of filtered water samples (to see if very small colloids differed from the bulk colloids) were inconclusive because of very low colloid concentrations.

b) The pH had no significant effect on the colloid stability. Increasing the pH caused the zeta potential to be slightly more negative, ranging from ~ -39 mV at pH 3.5 to ~ -46 mV at pH 8.3. The Chancellor colloids would be expected to be stable at all pHs measured at the NNSS (pHs higher than 8.3 would make the zeta potential more negative and further increase colloid stability).

c) Increasing the ionic strength from its natural value (I = 0.005 M) to I = 0.2 M using NaCl had no effect on the stability of the colloids (early stage coagulation rate ~ 0). Increasing the ionic strength above 0.2 M induced noticeable coagulation, and at I = 0.75 M, coagulation was rapid and the early stage coagulation rate remained almost constant above this ionic strength. This result indicates a critical coagulation concentration (CCC) between 0.7 and 0.8 M. The Chancellor colloids would be expected to remain stable at all ionic strengths reported at the NNSS.

d) Increasing the ionic strength induced a noticeable decrease in the zeta potential of the colloids, with the lowest values being observed at ionic strengths between 0.7 and 0.8 M, consistent with the above stability data. These ionic strengths significantly exceed any ionic strengths measured at the NNSS.

3.3 Mineralogy of the Chancellor Water Colloids

Figure 5 shows the XRD pattern obtained for a dried sample of the Chancellor water colloids. The sharp peaks in the pattern correspond to corundum (Al_2O_3) standard that was added to the sample at 20 wt%. The pattern provides only qualitative information on the mineralogy, although there are several weak or broad peaks that are suggestive of either illite or smectite or a combination of the two clays (indicated with arrows in Figure 5). The quality of the XRD pattern was likely degraded by the presence of the vacuum grease used to keep the very fine colloids from dispersing and creating a radiological hazard. Additional work with the sample would be required to differentiate smectite from illite (e.g., exposing the sample to different solutions, including glycol, to swell the smectite while leaving the illite unchanged). The elevated background in the pattern also suggests the presence of a significant amount of amorphous materials in the sample. Kersting and Zavarin (2011) reported the presence of zeolites and feldspar in Chancellor water colloids, but the presence of these minerals could not be deciphered from the qualitative XRD patterns obtained for the present study.

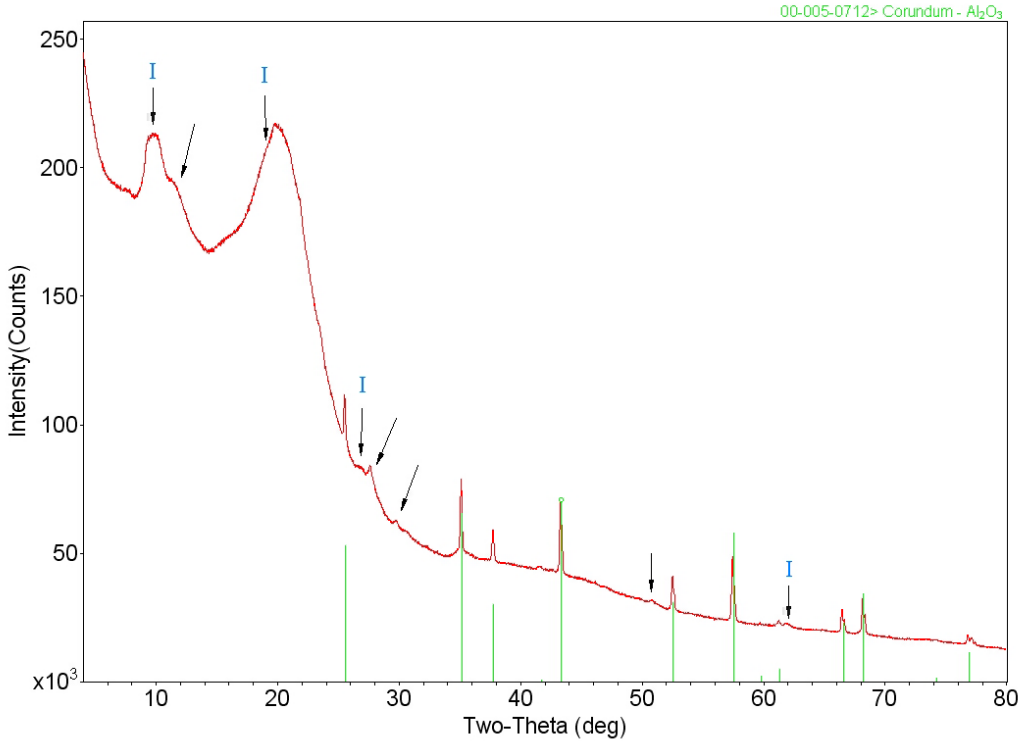

Figure 5. XRD analysis results of Chancellor water colloids. Arrows (I's) indicate locations of characteristic illite or smectite peaks. Green lines are associated with corundum standard.

3.4 Radionuclide Associations with Chancellor Water Colloids

3.4.1 ^{137}Cs Association with Chancellor Colloids in Unspiked Water

Figure 6 shows the alpha-beta liquid scintillation spectra of both unfiltered and filtered samples taken from an unstirred Chancellor water drum. These spectra were obtained using a Perkin-Elmer Tri-Carb 2500 scintillation counter, which lacked the high precision at low count rates of the Quantulus counter. The background spectrum of a water sample from well J-13 in NNSS Area 25 is also shown for comparison. This water has similar chemistry to Chancellor water but is known to be free of anthropogenic radioactivity, so it was considered to be a good water to use for NNSS background corrections. It is apparent in Figure 6 that filtration did not cause a significant change in the shape of the Chancellor water spectrum, although the counts are clearly decreased for the filtered sample relative to the unfiltered sample. Other than the very high count rates at low energies (not shown in Figure 6), which are indicative of tritium, the spectra indicate a predominance of ^{137}Cs activity in the water. ^{137}Cs has a characteristic double-humped spectrum (inset a of Figure 6) that coincides almost exactly with the unfiltered and filtered water spectra (other than at very low energies). This result is consistent the findings of Rose et al. (2011), who reported that ^{137}Cs was the dominant fission product in Chancellor water. Inset b of Figure 6 shows the ratio of the background-corrected unfiltered counts to background corrected filtered counts between 19 and 400 keV (avoiding the low-energy tritium that dominates the spectra below 18 keV). The relatively consistent ratio close to 2 indicates that approximately 50% of the ^{137}Cs was removed from the filtered sample and thus was associated with the colloids.

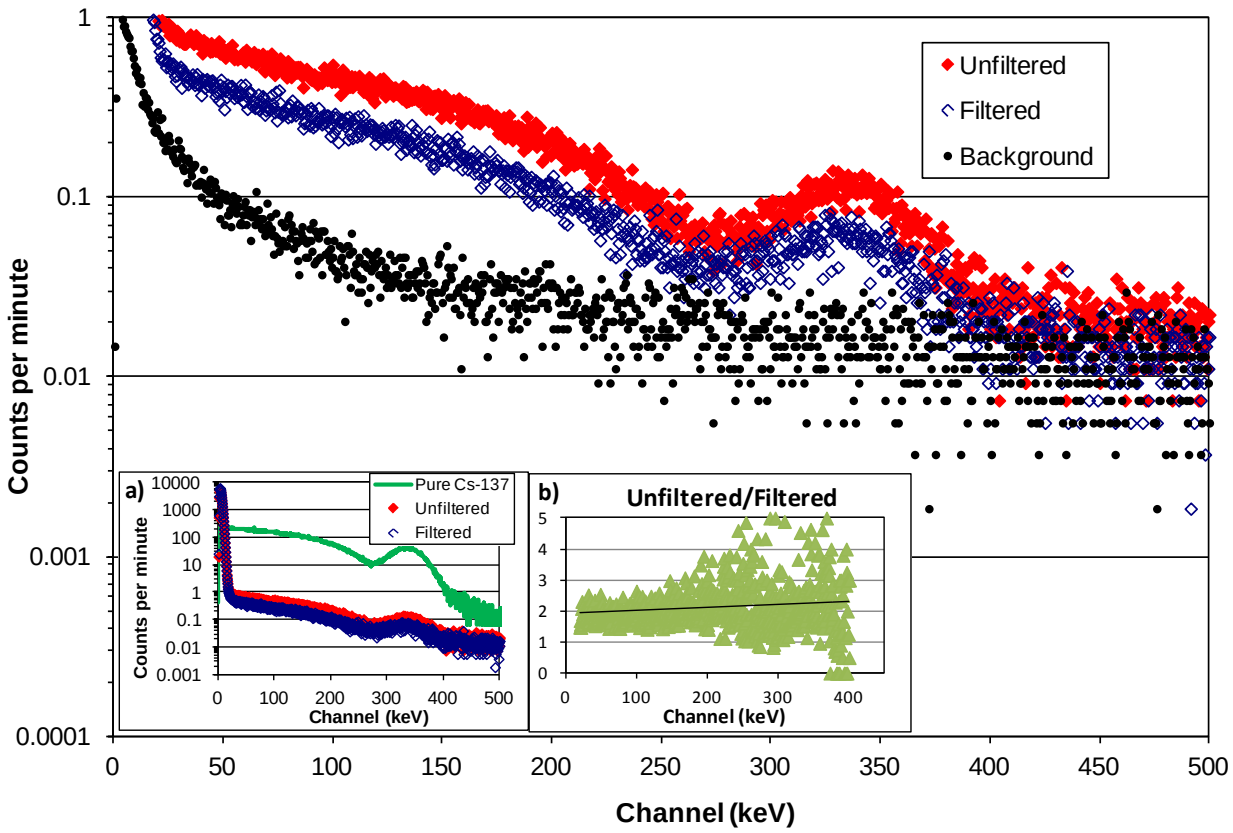

Figure 6. Liquid scintillation spectra of unfiltered and filtered Chancellor water and NNSS UE-25 J-13 water, used as a background. Inset a shows the spectrum of a much-higher concentration ^{137}Cs sample compared to the Chancellor water, and inset b shows the ratios of the background-corrected unfiltered to filtered counts/minute for the Chancellor water.

Figure 7 shows the beta-alpha liquid scintillation spectra obtained after ultracentrifugation of unfiltered Chancellor water samples, including spectra for the supernatant, the bottom 5 ml of the centrifuge tube after centrifugation, and a sample prior to centrifugation. The bottom 5 ml is enriched in ^{137}Cs relative to the sample before centrifugation because it contains all the colloids to which about 50% of the ^{137}Cs was adsorbed. These spectra were obtained using the Quantulus scintillation counter (note that the Quantulus allows clear delineation of a ^{137}Cs peak at around 70 keV that was not apparent in the Tri-Carb 2500 spectra of Figure 6). The spectra of Figure 7 are shifted to lower energies than the spectra of Figure 6, which we attribute to an inconsistency in the translation from channel number to keV on the two instruments. The spectra of Figure 7 also show a slight shift toward lower energies when colloids are present in the water, particularly for the higher-energy peak. This result might be attributable to slight differences in the ratios of water to scintillant in the samples, which affects the sample quench and thus the energies corresponding to peaks in the spectra. However, it is also possible that the colloids may have slightly attenuated the scintillation bursts that the counter detects, which would have shifted the peaks to lower energies.

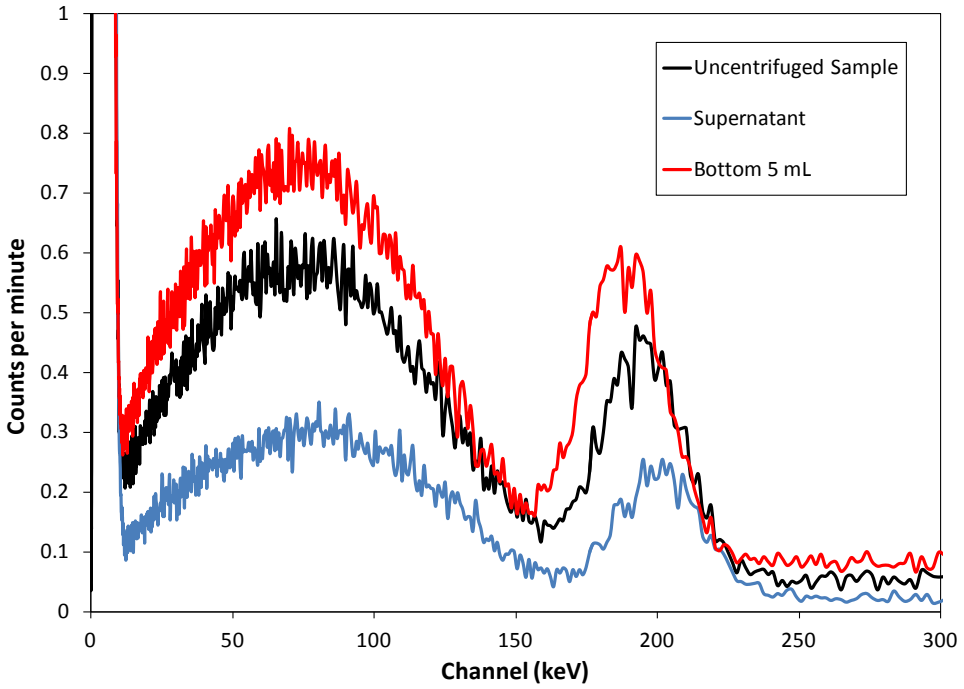

Figure 7. Total activity in stirred samples before and after centrifugation at 55K rpm for 1.5 hours. Activities are per 5 g of water sample. Bottom 5 mL refers to a sample taken from the bottom half of the sample tube after centrifugation.

It is apparent from Figure 7 that at any energy between about 20 keV and 250 keV, the ratio of counts in the uncentrifuged sample to counts in the supernatant sample is about 2, which is consistent with the results obtained for the unfiltered and filtered samples using the Tri-Carb 2500 scintillation counter. Thus, both ultrafiltration and ultracentrifugation and the use of two different liquid scintillation counters yielded essentially the same ^{137}Cs partitioning results; i.e., about 50% of the ^{137}Cs was associated with the colloids and the other 50% was in solution. Also, the absolute ^{137}Cs activities measured in the water samples were in excellent agreement with each other using the two separation methods and the two scintillation counters: about 34 dpm/ml for the unfiltered/ uncentrifuged water and about 17 dpm/ml for the filtered water or supernatant. These activities translate to concentrations of about 15,600 pCi/L and 7800 pCi/L, respectively, which for the unfiltered/uncentrifuged water is about 3.5 times lower than that given by Rose et al. (2011) and about 2 times lower than that given by Reimus et al. (2006). These discrepancies cannot be explained by radioactive decay; we do not have a good explanation for the wide range of values. However, the 50% partitioning of ^{137}Cs to the colloids measured for this study is in excellent agreement with the 50% partitioning reported by Reimus et al. (2006), so even though the absolute concentrations of ^{137}Cs reported by Reimus et al. (2006) were about twice those reported here, the partitioning of ^{137}Cs between colloids and solution are essentially identical. Given the colloid mass concentration of 120 mg/L in the water, the ~50% partitioning of ^{137}Cs translates to an estimated partition coefficient, or K_d value, of ~8.3×10^3 ml/g for the ^{137}Cs on the colloids. K_d values of this magnitude are not unusual for clays (e.g., Tamura, 1972; Comans et al., 1989). We expect that the predominant mechanism for ^{137}Cs adsorption to the colloids was cation exchange.

The $^{239/240}$Pu concentration in unfiltered Chancellor water, as reported by both Reimus et al. (2006) and Rose et al. (2011), is approximately 23 pCi/L, which translates to about 0.05 dpm/ml. As stated in Section 2.10, this activity level is nearly 3 orders of magnitude lower than the ^{137}Cs activity levels in the unfiltered water. Thus, although the activity of $^{239/240}$Pu in the Chancellor water was higher than in any other NNSS cavity water that has been analyzed to date, it was still too low to be analyzed by liquid scintillation counting.

3.4.2 Cs Association with Chancellor Colloids in Cs-Spiked Water

The dissolved Cs spike added to the Chancellor water increased the ^{137}Cs concentration from 1.56×10^{4} pCi/L to 1.84×10^{4} pCi/L, but the overall Cs concentration was increased from 1.30×10^{-12} M to 2.24×10^{-7} M, or approximately 5 orders of magnitude. Centrifugation of the spiked solution at 20-hr intervals at 16100 RPM for 15 min indicated that equilibrium partitioning of Cs between the colloids and solution phase was rapidly established. However, the separation of the colloids from the solution phase was incomplete under these centrifugation conditions, so quantitative Cs partitioning data were not obtained. An aliquot of the spiked solution that was used as the first injection solution into the column experiment was centrifuged at 55,000 RPM (~170,000 g) for 90 minutes, and the apparent partitioning of ^{137}Cs to the colloids was found to be about 54%, which is in excellent agreement with the results for the unspiked water. Thus, it was concluded that the addition of the Cs spike did not noticeably alter the partitioning of ^{137}Cs to the colloids, which suggests that there was a sufficient number of Cs sorption sites on the colloids that all of the spiked Cs could be readily accommodated without affecting the apparent colloid-solution partitioning.

The partitioning of ^{137}Cs to the Chancellor colloids was determined by centrifugation for each of the successive injection solutions in the column experiments. However, the measurements for the second and third injections weren't conducted until a few months after the injections, so it is possible that some Cs desorption from the colloids may have occurred in the intervening time for these injection solutions. Table 4 lists the partitioning results as well as an estimate of the Cs partition coefficient to the colloids in each solution (based on the fraction of Cs associated with colloids and the estimated colloid mass concentrations in the solutions). It is apparent that the partition coefficients increased dramatically with each successive injection solution in the multiple-injection column experiments despite the extra time allowed for desorption to occur in the case of the second and third injections. It is possible that the ^{137}Cs fraction adsorbed to the colloids at the time of the second and third injections was actually close to 1.0 or 100% adsorbed. These results suggest that the ^{137}Cs remaining adsorbed to the colloids after each pass through the column was more and more strongly associated with the colloids.

Table 4. ^{137}Cs partitioning to colloids and apparent K_d values on colloids in each of the Cs column injection solutions.

Solution	Total Cs conc., M	Fraction ^{137}Cs on colloids	^{137}Cs K_d value, ml/g
Unspiked Chancellor water	1.3×10^{-12}	0.50	8,300
Spiked injection solution 1	2.24×10^{-7}	0.54 ± 0.05	13,100
Spiked injection solution 2	2.67×10^{-8}	0.83 ± 0.05	61,600
Spiked injection solution 3	1.46×10^{-8}	0.91 ± 0.05	239,600

3.4.3 $^{239/240}$Pu Association with Chancellor Colloids in Pu-Spiked Water

The Chancellor water was spiked with a solution containing $^{239/240}$Pu(IV) intrinsic colloids (Sections 2.11 and 2.12.2.2) to approximately 0.63 μg/L, or 2.63 x 10^{-9} M, to allow quantification by liquid scintillation counting in the column transport experiments without ^{137}Cs interference. The association of $^{239/240}$Pu with the natural colloids was determined by centrifugation (see below) immediately after Pu addition, at the time of the first column injection, and after 6 months of aging. The Pu partitioning to the natural colloids was also determined in the second and third injection solutions in the column experiments, although these samples were not measured until a few months after the injections. As noted in Section 2.11, the Pu(IV) intrinsic colloids were much smaller than the natural Chancellor water colloids, and the association of the Pu(IV) colloids with the natural colloids could be determined by taking advantage of their size differences (discussed in next paragraph).

The $^{239/240}$Pu association with the natural colloids was determined by separation of the natural colloids by centrifugation and counting the activity associated with the supernatant. However, unlike the Cs partitioning measurements, high-speed centrifugation was avoided because we did not want to spin down the Pu(IV) intrinsic colloids with the Chancellor colloids. Instead, the spiked solution was centrifuged at the modest speed of 5000 RPM. Immediately after spiking the Chancellor water with the intrinsic Pu(IV) colloids, twenty four 2-ml samples were collected and centrifuged at this speed. The centrifuge was stopped at 10 min intervals, and the supernatant from two of the samples was removed to measure for $^{239/240}$Pu activity using liquid scintillation counting. Figure 8 shows the fraction of Pu removed from solution at each 10-minute time interval. Figure 9 shows the same information after 6 months of aging of the spiked Chancellor water. A control sample consisting of the freshly-prepared Pu(IV) intrinsic colloid spike solution was centrifuged under the same conditions at each time, and it was found that the amount of $^{239/240}$Pu removed from the supernatant in this sample was negligible at all 10-minute intervals. However, about 95% of the $^{239/240}$Pu was removed from the spike solution

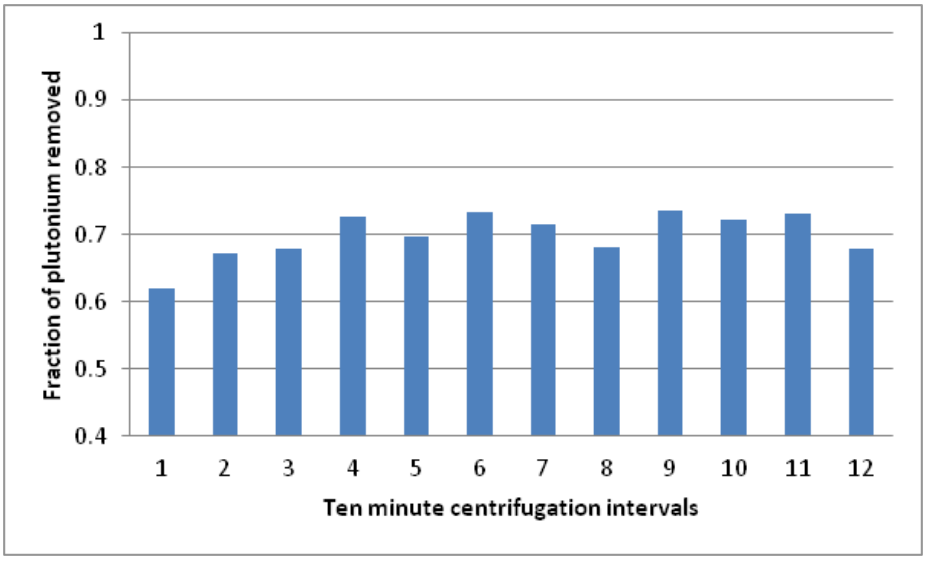

Figure 8. Fraction of Pu removed from supernatant at 10 minute intervals for freshly-prepared $^{239/240}$Pu-spiked Chancellor water. Centrifugation speed was 5000 RPM.

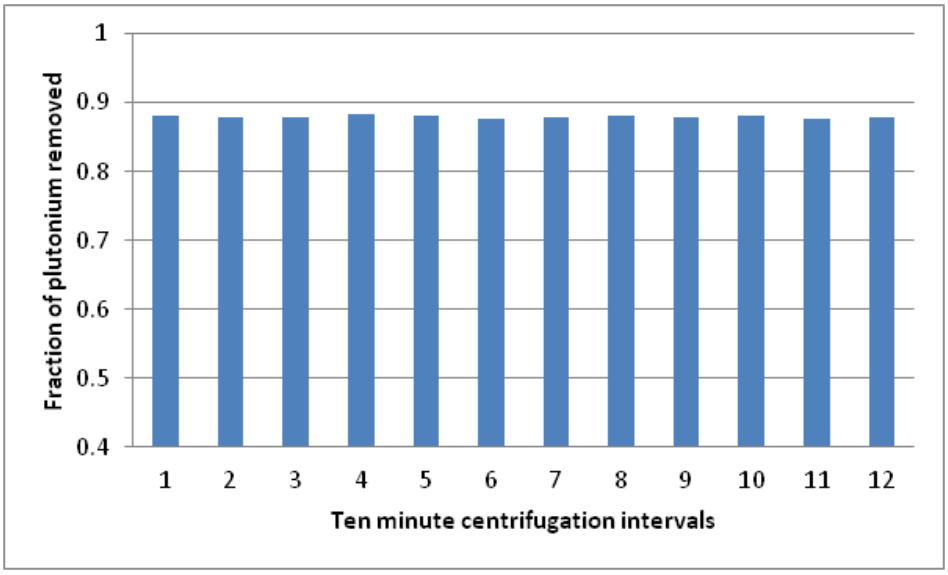

Figure 9. Fraction of Pu removed from supernatant at 10 minute intervals for 6-month-aged $^{239/240}$Pu-spiked Chancellor water. Centrifugation speed was 5000 RPM.

when high-speed centrifugation (55,000 RPM for 90 minutes) was employed. After six months of aging, high-speed centrifugation was less efficient at removing the $^{239/240}$Pu from this spike solution, suggesting that some of the Pu(IV) intrinsic colloids likely transformed to solute Pu(IV) or Pu(V) that could not be removed by centrifugation.

The data of Figures 8 and 9 indicate that a stable Pu partitioning factor between the natural colloids and the solution phase (i.e., dispersed Pu(IV) intrinsic colloids) was achieved quite rapidly at 5000 RPM. The average fraction of Pu associated with natural colloids in the freshly-prepared spiked solution leveled off at 0.71 ± 0.02 after 30 min of centrifugation. Partitioning to colloids of 0.88 ± 0.02 was measured after the first 10-min interval for the 6-month-old spiked solution and remained unchanged after all subsequent 10-min intervals.

It was recognized that the 5000 RPM centrifugations were probably not completely effective at removing the natural colloids from solution. To evaluate the effectiveness, the colloid concentrations and size distributions in supernatant samples of the centrifuged Chancellor water were measured at 10-min intervals using the in-situ laser particle spectrometer. The results are shown in Figure 10. It is apparent that the vast majority of the natural colloids were removed after three 10-min intervals, but there was a persistence of smaller diameter colloids even after 40 minutes. Based on these results and the results of Figures 8 and 9, it was decided that centrifuging at 5000 RPM for 30 minutes was an optimal centrifugation time to determine partitioning of Pu(IV) intrinsic colloids to the natural colloids.

The $^{239/240}$Pu partitioning to the natural colloids measured in each of the column injection solutions using the method described above is listed in Table 5. The interpretation of these partitioning results is complicated by the complex speciation behavior of Pu. It is probably misleading to say that these results represent the partitioning of strictly Pu(IV) intrinsic colloids to the Chancellor colloids because the Pu(IV) colloids likely partially transformed into Pu(IV) and Pu(V) solute species, particularly after a few months of sitting in sample containers before

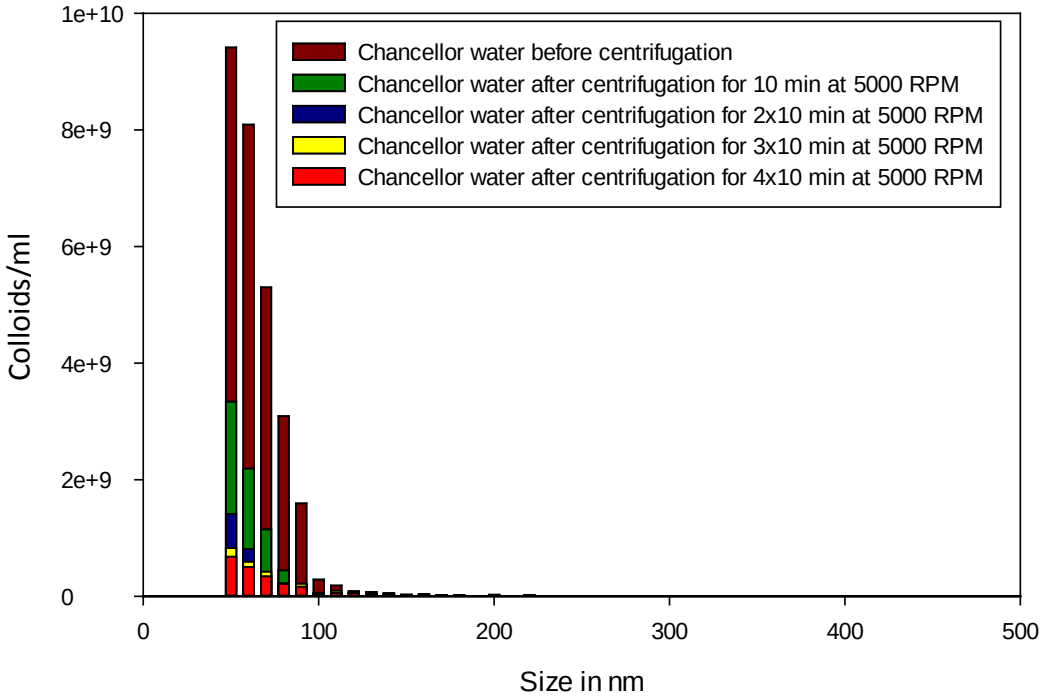

Figure 10. Colloids/ml in different size bins as a function of centrifugation time as determined by in-situ laser particle spectrometer. Centrifugation was performed at 5000 RPM.

Table 5. $^{239/240}$Pu partitioning to colloids and apparent K_d values on colloids in each of the Pu column injection solutions.

Solution	Total Pu conc., M	Fraction Pu on colloids	Pu K_d value, ml/g
Injection solution 1	2.64×10^{-9}	0.83 ± 0.05	60,600
Injection solution 2	2.26×10^{-9}	0.92 ± 0.05	202,200
Injection solution 3	1.26×10^{-9}	0.97 ± 0.05	507,300

being analyzed (injection solutions 2 and 3). Nevertheless, it is apparent that the Pu partitioning to the colloids tended to increase significantly with each column injection, and it was considerably greater in the third injection solution than in the original unspiked Chancellor water, suggesting that the Pu remaining associated with the natural colloids after each pass through the column was more and more strongly associated with the natural colloids. In this regard, the Pu adsorption behavior was similar to the Cs behavior despite the fact that the adsorption mechanisms for the two species are almost certainly much different (intrinsic colloid attachment and/or redox-mediated surface complexation for Pu as opposed to cation exchange for Cs).

The speciation of Pu in the first column injection was assumed to be dominated by Pu(IV) intrinsic colloids (either associated with natural Chancellor colloids or dispersed in the solution phase). However, a small fraction of the Pu was likely to have been present in the Pu(V) oxidation state and as dissolved Pu(IV). The transformation of the Pu(IV) intrinsic colloids to solute Pu(IV) and Pu(V) (either in solution or adsorbed to the Chancellor colloids) almost certainly occurred over time in the experiments. The concentrations of Pu were too low to allow for speciation determination by spectroscopic methods. Several excellent reviews have been

published recently to address the complexity of plutonium solution speciation (e.g., Neck, 2007), and these were used to guide the interpretations of the Pu column experiment results.

3.5 Column Transport Experiments

3.5.1 Unspiked Chancellor Water Experiment

The breakthrough curves of ^{3}HHO, colloids, and ^{137}Cs in the unspiked column transport experiment and the model fits to the curves are shown in Figure 11. The concentrations of each constituent exiting the column were normalized by dividing the measured concentration by the constituent concentrations in the unfiltered Chancellor water (i.e., the injection concentrations). Figure 12 shows the normalized colloid breakthrough curve adjusted downward to have approximately the same maximum concentration as the ^{137}Cs breakthrough curve. The coincidence of the colloid and ^{137}Cs curves, and the fact that both have an earlier breakthrough and earlier decrease than the ^{3}HHO breakthrough curve (because of increased dispersion and some size exclusion of the colloids relative to the ^{3}HHO), strongly suggests that the ^{137}Cs exiting the column was associated with colloids that transported through the column.

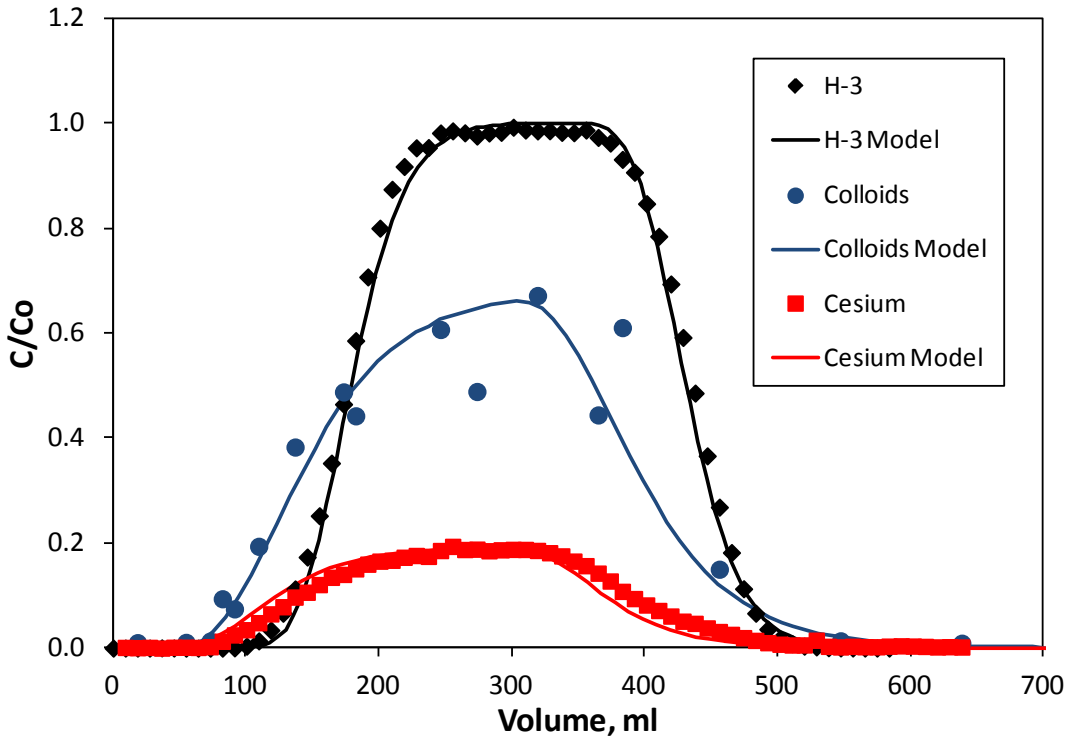

Figure 11. Breakthrough curves and model fits for the unspiked Chancellor water column experiment. Concentrations are normalized to injection concentrations. See Table 6 for best-fitting model parameters.

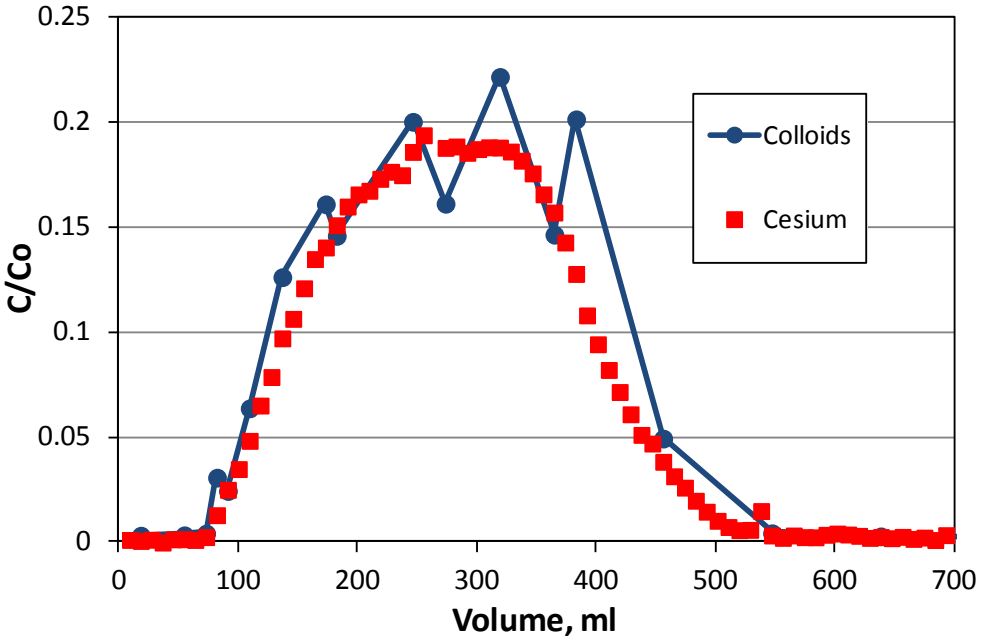

Figure 12. Breakthrough curves of Chancellor colloids and ^{137}Cs in unspiked water column experiment with colloid C/Co adjusted downward to match ^{137}Cs C/Co.

Table 6. Best-fitting model parameters for the unspiked Chancellor water column experiment.

Parameter	Value
Colloid Recovery (calc.)	0.67 (67%)
^{137}Cs Recovery (calc.)	0.20 (20%)
^{3}HHO mean res. time, hr	50
^{3}HHO Peclet number	62
Colloid mean res. time, hr	45
Colloid Peclet number	12
Colloid filtration rate constant, k_{fc}, hr^{-1}	0.0089
^{137}Cs desorption rate constant from colloids, k_{rsc}, hr^{-1}	0.014

The best-fitting model parameters for the breakthrough curves of Figure 11 are listed in Table 6. The best fits were obtained assuming no transport of the ^{137}Cs that was initially dissolved in the Chancellor water (~50% of the total ^{137}Cs), implying very rapid and irreversible sorption of this fraction to the tuff in the column. Of the remaining ~50% of the ^{137}Cs that was initially associated with colloids, only 67% of this mass, or 33% of the total ^{137}Cs in the injection pulse, would have been expected to transport through the column if ^{137}Cs did not desorb at all from the colloids because the colloid recovery was only 67%. However, the fact that only 20% of the total ^{137}Cs in the injection pulse was recovered suggests that about 1/3rd of the colloid-associated ^{137}Cs in the pulse desorbed from the colloids as a result of competitive sorption processes in the column. The values of k_{fc} and k_{rsc} in Table 6 reflect the values necessary to have ~67% of the

colloids filtered irreversibly in the column and ~33% of the colloid-associated ^{137}Cs desorbed from the colloids and become irreversibly adsorbed to the tuff in the column.

3.5.2 Cs-Spiked Chancellor Water Experiments

The breakthrough curves of ^{3}HHO, colloids, and ^{137}Cs after each of the three injections in the Cs-spiked column transport experiments and the model fits to the curves are shown in Figures 13, 14, and 15. The model parameters yielding the best fits to the data are listed in Table 7. The ^{137}Cs mass fractions associated with the Chancellor colloids in each of the injection solutions, as measured by ultracentrifugation, are also listed in Table 7.

A few key observations are apparent from Figures 13, 14, and 15 and Table 7:

- The colloids were not completely recovered after the first column injection, but their recoveries were essentially 100% for the second and third injections. Also, the first arrival time of the colloids tended to decrease for each successive injection. The fact that the best-fitting mean residence time and Peclet number of the colloids were always smaller than the corresponding ^{3}HHO parameters (Table 3) is attributed to size exclusion and increased hydrodynamic dispersion of the colloids relative to a conservative solute.

- The colloid recovery after the first injection was significantly higher than the colloid recovery in the unspiked Chancellor water experiment (92% vs. 67%). We suspect that the colloid concentrations measured in the column effluent samples in the unspiked experiment may have been low because these samples were stored for several weeks

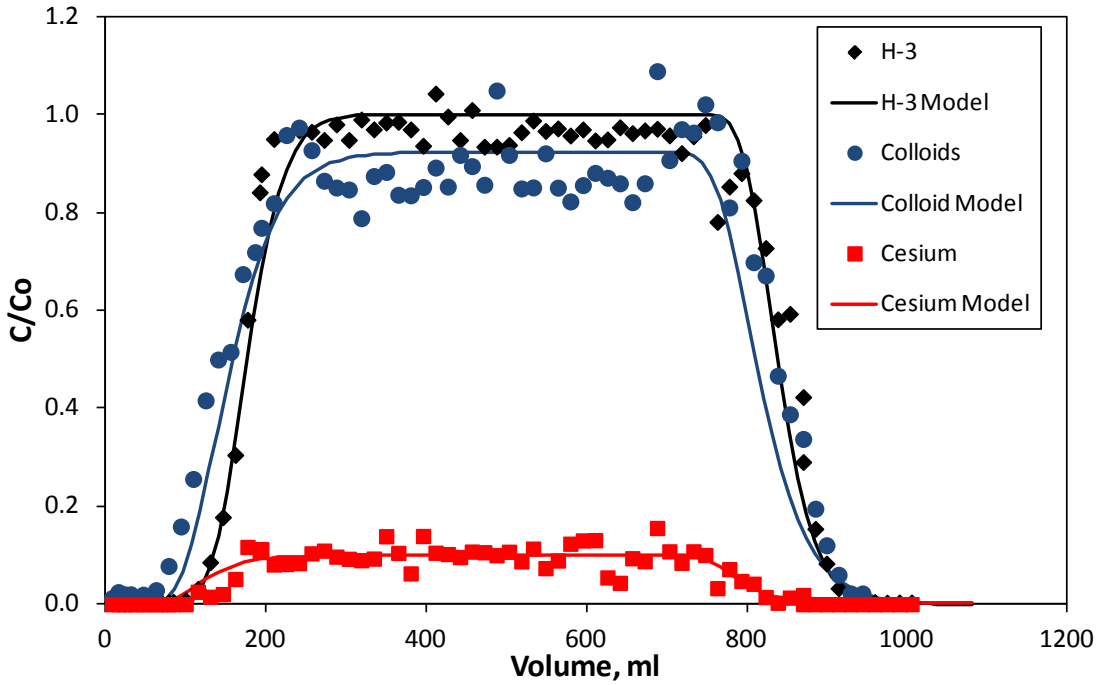

Figure 13. Breakthrough curves and model fits for the first injection in the Cs-spiked Chancellor water column experiment. Concentrations are normalized to injection concentrations. See Table 7 for best-fitting model parameters.

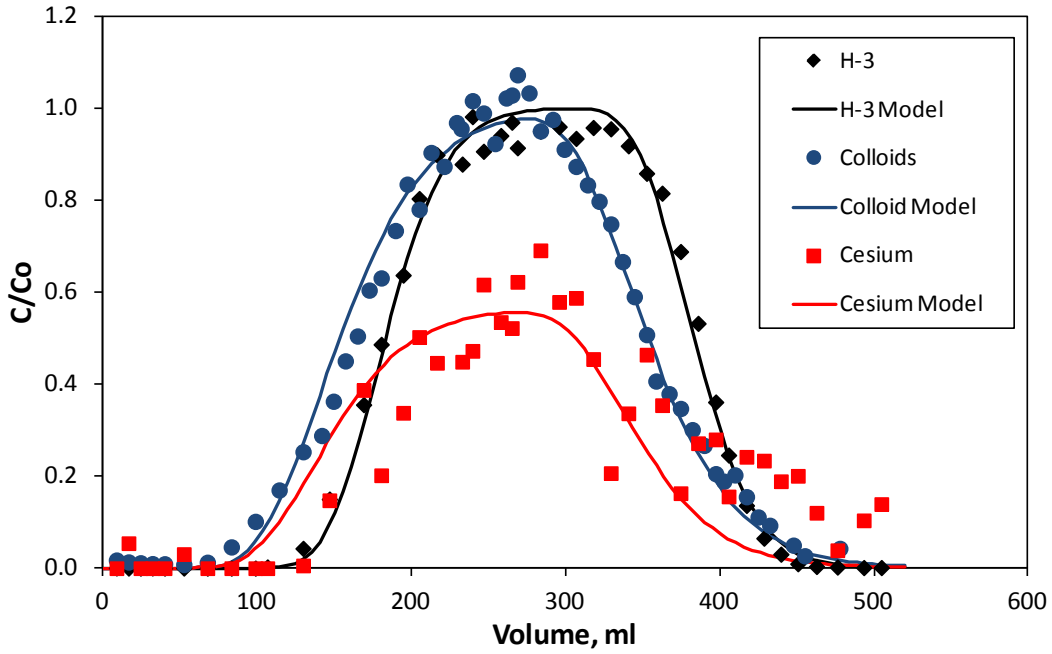

Figure 14. Breakthrough curves and model fits for the second injection in the Cs-spiked Chancellor water column experiment. Concentrations are normalized to injection concentrations. See Table 7 for best-fitting model parameters.

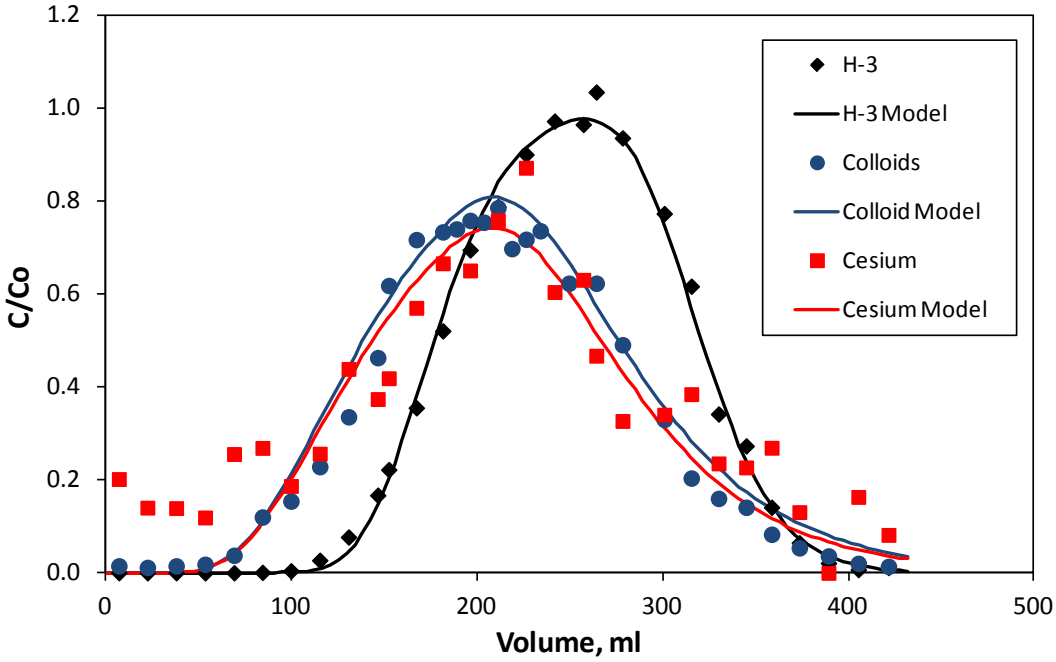

Figure 15. Breakthrough curves and model fits for the third injection in the Cs-spiked Chancellor water column experiment. Concentrations are normalized to injection concentrations. See Table 7 for best-fitting model parameters.

Table 7. Best-fitting model parameters for the Cs-spiked Chancellor water column injections.

Parameter	Injection 1	Injection 2	Injection 3
Colloid Recovery (calc.)	0.92 (92%)	~100%	~100%
^{137}Cs Recovery (calc.)	0.10 (10%)	0.62 (62%)	>0.95 (95+%)
^{3}HHO mean res. time, hr	50	93	50
^{3}HHO Peclet number	46	71	61
Colloid mean res. time, hr	45	80	42
Colloid Peclet number	19	25	11
Colloid filtration rate constant, k_{fc}, hr^{-1}	0.0018	0	0
^{137}Cs desorption rate constant from colloids, k_{rsc}, hr^{-1}	0.033	0.0048-0.0073*	0.0009-0.0023*

* First number assumes that fraction ^{137}Cs adsorbed to colloids in injection solution is the fraction given in Table 4; second number assumes 100% ^{137}Cs sorption to colloids in injection solution.

before they were measured by the in-situ laser spectrometer, whereas the samples collected for the spiked water experiment were analyzed almost immediately. It is also possible that the injected colloid concentrations in the unspiked water experiment were measured erroneously high, as the colloid concentrations exiting the column in both experiments were in reasonable agreement with each other but the injection concentration in the unspiked experiment was reported to be about 30% higher than in the spiked experiment. If both experiments had approximately the same injection concentrations, their colloid recoveries would have been similar.

- Despite the apparent higher recovery of the colloids after the first injection in the spiked experiment relative to the unspiked experiment, the ^{137}Cs recovery after the first injection in the spiked experiment was considerably lower than in the unspiked experiment, suggesting that the ^{137}Cs in the spiked water desorbed more readily from the colloids than the ^{137}Cs in the unspiked water (even though approximately the same fraction of ^{137}Cs was adsorbed to the colloids in both waters). Whereas approximately 1/3rd of the colloid-associated ^{137}Cs was deduced to desorb from the colloids in the unspiked experiment, about 3/4^{ths} of the colloid-associated ^{137}Cs was deduced to desorb from the colloids after the first injection in the spiked experiment. This difference might be attributable to the substantially higher Cs concentration that was spiked into the latter experiment, which although it did not appear to affect the overall partitioning of ^{137}Cs to the colloids, may have caused some ^{137}Cs to be displaced from the stronger sorption sites on the colloids and thus be more susceptible to desorption during the first column injection.

- The ^{137}Cs recovery after each successive injection in the spiked-water experiments steadily increased, with the recovery of the ^{137}Cs being nearly 100% after the third injection. Some of this result is attributable to the increased mass fraction of ^{137}Cs associated with colloids in each successive injection, which is not surprising given that only colloid-associated ^{137}Cs was deduced to be exiting the column. However, it is also attributable to the significant decrease in the apparent desorption rate constant of the ^{137}Cs from the colloids with each successive injection, which suggests that the ^{137}Cs that

remained adsorbed to the colloids after each injection was, on average, more strongly associated with the colloids than in the previous injection.

3.5.3 $^{239/240}$Pu-Spiked Chancellor Water Experiments

The breakthrough curves of ^{3}HHO, colloids, and $^{239/240}$Pu after each of the three injections in the Pu-spiked column transport experiments and the model fits to the curves are shown in Figures 16, 17, and 18. The model parameters yielding the best fits to the data are listed in Table 8. The Pu mass fractions associated with the Chancellor colloids in each of the injection solutions, as measured by ultracentrifugation, are also listed in Table 8. Note that the desorption rate constant of the $^{239/240}$Pu from the colloids for the first injection (Figure 16) had to be decreased with time during the injection to obtain a good match to the $^{239/240}$Pu breakthrough curve because of the steady increase in normalized Pu concentrations instead of a plateau after the initial breakthrough, as was observed for the colloids. The only way this steady increase could be accounted for was to assume that the Pu desorption rate constant from the colloids decreased with time. However, it is also possible that the increase could be attributed to the breakthrough of a fraction of the Pu(IV) nanocolloids that were not associated to the Chancellor colloids.

The key observations from Figures 16, 17, and 18 and Table 8 are:

- Similar to the Cs-spiked column experiments, the Chancellor colloids were not completely recovered after the first column injection, but their recoveries were essentially 100% for the second and third injections. Also, the colloid recovery after the first

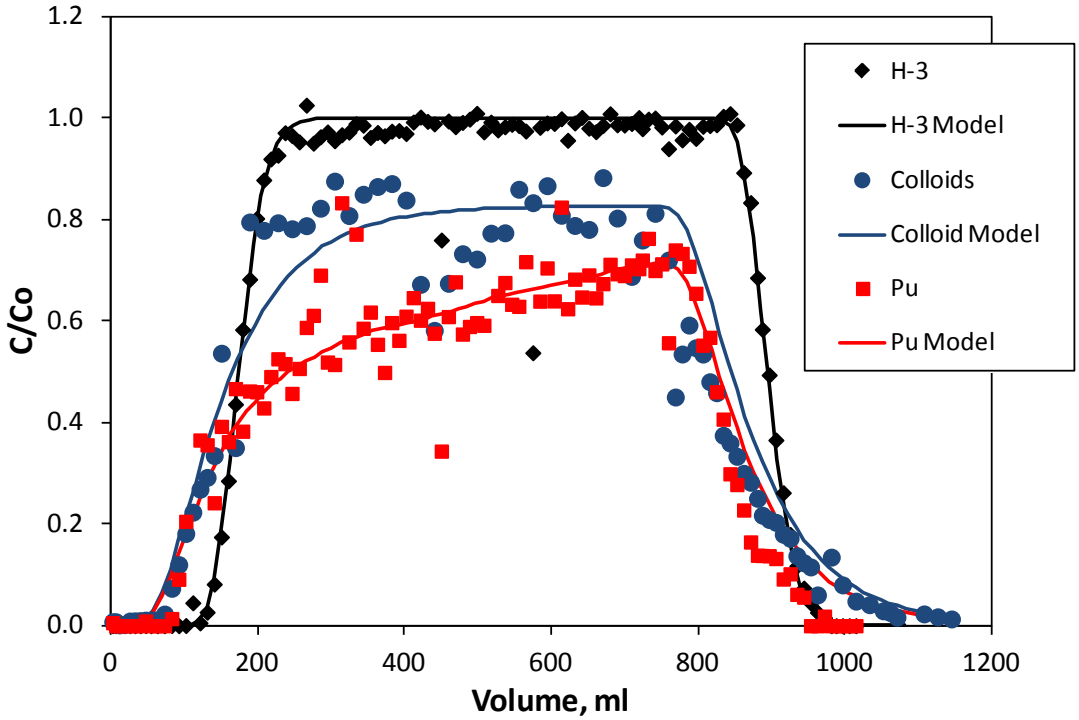

Figure 16. Breakthrough curves and model fits for the first injection in the Pu-spiked Chancellor water column experiment. Concentrations are normalized to injection concentrations. See Table 8 for best-fitting model parameters.

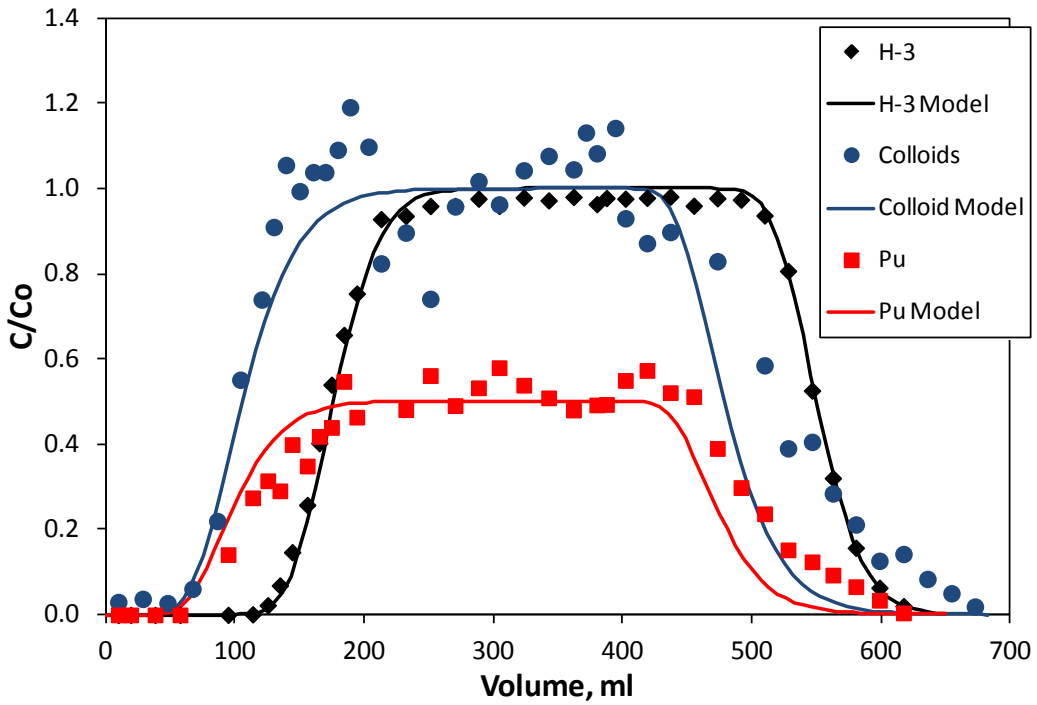

Figure 17. Breakthrough curves and model fits for the second injection in the Pu-spiked Chancellor water column experiment. Concentrations are normalized to injection concentrations. See Table 8 for best-fitting model parameters.

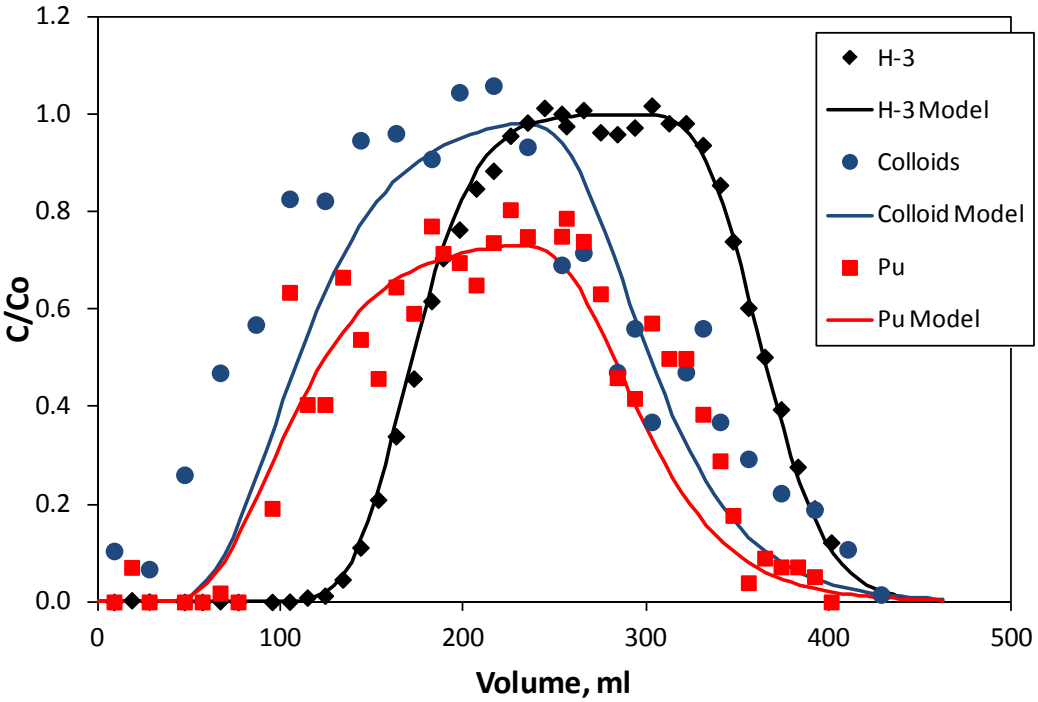

Figure 18. Breakthrough curves and model fits for the third injection in the Pu-spiked Chancellor water column experiment. Concentrations are normalized to injection concentrations. See Table 8 for best-fitting model parameters.

Table 8. Best-fitting model parameters for the $^{239/240}$Pu-spiked Chancellor water column injections.

Parameter	Injection 1	Injection 2	Injection 3
Colloid Recovery (calc.)	0.82 (82%)	~100%	~100%
$^{239/240}$Pu Recovery (calc.)	0.62 (62%)	0.53 (53%)	0.79 (79%)
^{3}HHO mean res. time, hr	49	55	49
^{3}HHO Peclet number	76	80	82
Colloid mean res. time, hr	49	34	33
Colloid Peclet number	6	20	15
Colloid filtration rate constant, k_{fc}, hr^{-1}	0.004	0	0
$^{239/240}$Pu desorption rate constant from colloids, k_{rsc}, hr^{-1}	0.004 (1st 50 hr)* 0.002 (2nd 50 hr) 0.001 (3rd 50 hr) 0 (4th 50 hr)	0.018-0.021**	0.0083-0.0093**

* For injection 1, the $^{239/240}$Pu desorption rate constant had to decrease as indicated over the 200 hour duration of the injection to match the $^{239/240}$Pu breakthrough curve.

** First number assumes that fraction $^{239/240}$Pu adsorbed to colloids in injection solution is the fraction given in Table 5; second number assumes 100% $^{239/240}$Pu sorption to colloids in injection solution.

injection was considerably higher than in the unspiked water experiment, and the first arrival time of the colloids tended to decrease with each successive injection. Both the apparent first arrival time and recovery of the colloids after the third injection (Figure 18) were unrealistic in that the first arrival time was much earlier than in any other experiment and the colloid recovery was calculated to be greater than 100% (the model curve in Figure 18 corresponds to 100% recovery). The most likely explanations for this behavior are that (1) some non-injected colloids were mobilized in the column by a flow transient early in this experiment, (2) the laser particle spectrometer was measuring an unusually high background early in the experiment or (3) the early samples were contaminated somehow with colloidal-sized particles. The lack of Pu associated with this apparent early colloid arrival suggests that the early colloids, if real, were likely not colloids from previous injections that had been filtered in the column.

- The Pu recovery after the first injection was higher than after the second injection, which is contrary to what was observed for the spiked ^{137}Cs experiments. We do not have a definitive explanation for this behavior, but we suspect that it can be attributed to transformation of some of the Pu(IV) nanocolloids to either or both Pu(IV) and Pu(V) in solution, followed by re-partitioning of this dissolved material between the Chancellor colloids and the solution phase in the aftermath of the experiment. It is reasonable to expect that there would have been a driving force for dissolution/oxidation of the Pu(IV) nanocolloids after the first injection because the samples recovered from the column after this injection should have been almost entirely devoid of any solution phase Pu or of Pu(IV) nanocolloids that were not associated with Chancellor colloids. Despite the fact that the transformation of Pu resulted in greater partitioning of Pu to the colloids for the second injection (Table 5), the association of the Pu to the colloids was apparently

somewhat weaker during the second injection than during the first injection, which led to a somewhat larger deduced desorption rate constant for the Pu from the colloids than for the first injection.

- The Pu recovery after the third injection was higher than after the second injection, and the deduced desorption rate constant for Pu from the colloids was smaller than after the second injection (although it was comparable to the desorption rate constants deduced for the first injection). This result is qualitatively consistent with the observed behavior in the spiked ^{137}Cs experiments in that the Pu appears to be more strongly associated with the colloids in the third injection than in the second injection. The trend reversal after the first injection (a decrease in Pu association with colloids after the first injection, followed by an increase after the second injection) is likely attributable to a gradual stabilization of the Pu speciation over time, with the speciation probably being much more similar in the second and third injections than in the first and second injections. As stated above, we suspect that a transition was occurring from the Pu being predominantly Pu(IV) nanocolloids in the first injection to a mix that included much more solute Pu(IV) and Pu(V) in the second and third injections. Pu in the solution phase after the first injection would have been dominated by Pu(V) and Pu associated with the Chancellor colloids was likely dominated by Pu(IV) and perhaps some remaining Pu(IV) nanocolloids.

We note that in addition to measuring the colloid concentrations used to construct the breakthrough curves of Figures 11 through 18, the laser particle spectrometer also measured colloid size distributions in each column effluent sample that was analyzed (i.e., similar to the data of Figure 3). We looked for differences in the size distributions over time because of the greater colloid recoveries after the second and third injections, but the size distributions throughout the experiments were essentially indistinguishable from the starting Chancellor water. This result suggests that, at least within the ability to measure it, colloid size was not the attribute that resulted in preferential filtration of some of the colloids during the first injection. Rather, other features such as shape, mineralogy, or surface charge, or perhaps some combination of these must have been responsible for distinguishing the easily filtered colloids from the colloids that remaining unfiltered.

4. Discussion

While the properties of the Chancellor groundwater colloids and the partitioning of both ^{137}Cs and $^{239/240}$Pu to these colloids in the cavity water are certainly of interest, we consider the most significant results of this study to be the apparent decrease in both the colloid filtration rate constants and the desorption rate constants of ^{137}Cs and $^{239/240}$Pu from the colloids with each successive injection in the radionuclide-spiked column transport experiments. The re-injection of the recovered colloids and radionuclides into the same column two times was equivalent to conducting three column experiments in series, with breakthrough curves obtained at three different time and distance scales. The results suggest that there is a relatively rapid filtration of colloids that are susceptible to filtration and a relatively rapid desorption of radionuclides from ‘weaker’ sorption sites on colloids, but as time and distance scales increase, mobile colloids will be more likely to remain mobile and radionuclides adsorbed to colloids will be more likely to remain adsorbed to the mobile colloids. In effect, there appear to be processes occurring that

'naturally select' for more mobile colloids and more strongly colloid-associated radionuclides as time and distance scales increase.

Although the time and distance scales evaluated in this study are only a small fraction of the time and distance scales of interest for Corrective Action Unit (CAU) model predictions, the apparent trends mentioned in the previous paragraph are consistent with field observations such as the transport of colloids and colloid-associated radionuclides originating from the Benham cavity on Pahute Mesa to locations significant distances downgradient, like ER-20-5 and ER-20-7 (Kersting et al., 1999; Zavarin, 2012). Given that there was no appreciable Chancellor colloid filtration after the second injection into each laboratory column (i.e., a filtration rate indistinguishable from zero) and the recovery of ^{137}Cs after the third injection was essentially 100% of the colloid-associated ^{137}Cs in the injection solution (i.e., a desorption rate from the colloids indistinguishable from zero), a simple-minded extrapolation of the results of this study could lead to a prediction of several percent of the ^{137}Cs present in Chancellor water being able to transport over very long distances and times. Although there was still measurable desorption of Pu from the colloids after the third Pu injection, a similar conclusion might also be reached for the colloid-facilitated transport of $^{239/240}$Pu. The much greater association of Pu with the naturally-occurring Chancellor colloids as compared to the ^{137}Cs (90% vs. 50% association), and the fact that the laboratory experiments involved introducing Pu as Pu(IV) nanocolloids that likely underwent transformations that enhanced their dissociation from the colloids (at least initially), suggests that a significant fraction of Pu might transport over long time and distance scales.

Figure 19 shows the ^{137}Cs and $^{239/240}$Pu mass fractions having apparent desorption rate constants less than or equal to the corresponding values on the x-axis, as determined from the laboratory column experiments. The "less-than-or-equal-to" designation is used because any radionuclide mass deduced to desorb from colloids in any given injection experiment could have had a desorption rate constant greater than the rate constant estimated for the entire mass, but it could not have been less than this rate constant. Only one point is shown for the unspiked column experiment because there was only a single injection of the unspiked water. However, multiple points are plotted for the multiple-injection column experiments with the radionuclide-spiked waters. The points for the multiple injection experiments in Figure 19 effectively constitute portions of cumulative probability distributions of the estimated Cs and Pu desorption rate constants from the colloids. This plot shows that while a significant fraction of the radionuclide mass that was initially adsorbed to the colloids desorbed rather quickly in the columns, there was a substantial fraction of both Cs and Pu that remained adsorbed throughout the experiments and thus had much smaller apparent desorption rate constants.

The radionuclide masses that were originally in solution were not counted as part of the mass fractions in Figure 19. Thus, a mass fraction of 1.0 in the case of Cs in Figure 19 corresponds to the ~50% of the Cs mass that was originally adsorbed to the colloids. The remaining 50% of the Cs mass in the solution phase did not transport through the columns at all based on the experimental observations. For the Pu, the second injection solution was used as the initial condition for the mass fraction calculations (hence there are only two sets of points plotted for Pu instead of three). It was recognized that the Pu(IV) nanocolloids in the first injection probably partially dissolved and/or oxidized between the first and second injections, causing re-

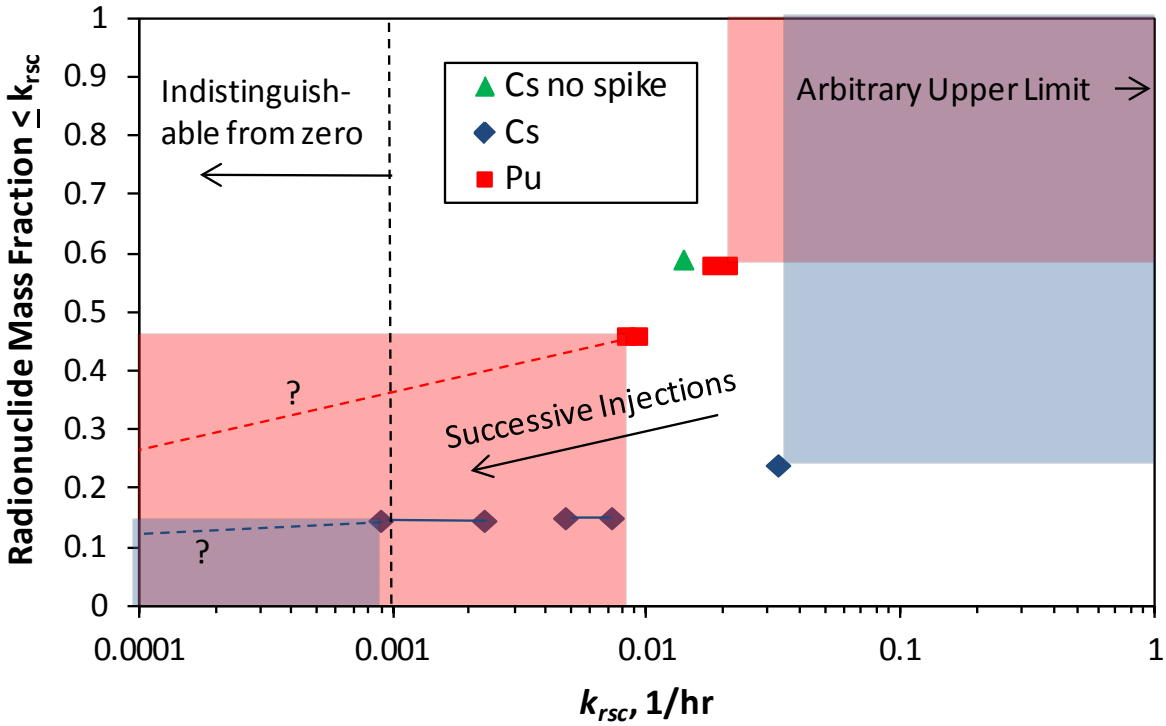

Figure 19. Cumulative mass fraction distributions of Cs and Pu desorption rate constants from Chancellor colloids deduced from the column transport experiments. Pink-shaded regions are regions of uncertainty for Pu desorption rate constants, and blue-shaded regions are regions of uncertainty for Cs desorption rate constants. See text for additional discussion.

equilibration and repartitioning of Pu between the colloids and solution, so the partitioning in the first injection was not used for the mass fraction basis. It was assumed that re-equilibration and repartitioning had come to near-completion by the time of the second injection, so the ~90% Pu adsorbed to the colloids in the second injection solution was used as the mass fraction basis. This assumption is consistent with the ~90% Pu association with colloids in the unspiked Chancellor water that was reported by both Reimus et al. (2006) and Rose et al. (2011).
The y-axis values in Figure 19 are calculated as the product of the recovered radionuclide mass fractions for all injections preceding the experiment from which the radionuclide desorption rate constant was estimated. For instance, the mass fraction associated with the Cs desorption rate constant of 0.0009 hr^{-1}, estimated from the last Cs injection, was calculated as (0.97)(0.63)(0.24) = 0.145, where,

0.97 = fractional mass recovery of Cs for third injection
0.63 = fractional mass recovery of Cs for second injection
0.24 = (fractional mass recovery of Cs for first injection)/[(fraction of Cs associated with colloids in the first injection solution)(fractional mass recovery of colloids for first injection)] = 0.113/[(0.5)(0.94)]

Dividing by the Cs fraction associated with colloids in the first injection (0.5) in the last calculation effectively eliminates the Cs mass that was originally in solution from the mass fraction calculations. Dividing by the fractional mass recovery of colloids for the first injection

(0.94) effectively accounts for the Cs mass lost as a result of colloid filtration after the first injection rather than from Cs desorption from colloids. There is no such correction for the second and third Cs injections because there was no apparent filtration of colloids associated with those injections (i.e., all Cs not recovered after those injections had to be a result of Cs desorption from the colloids, even if some of the desorption occurred before the injections started). Also, no corrections were necessary for the Pu mass fractions because there was no apparent filtration of colloids after the first injection (the second injection solution was used as the mass fraction basis).

The points that are connected by solid lines in Figure 19 are two different sets of calculations for both the second and the third injections for a given radionuclide. In the calculation that resulted in the larger desorption rate constant in each pair, it was assumed that the initial colloid-associated mass fraction of radionuclide in each injection solution was 1.0 instead of the value determined from ultracentrifugation (the values given in Tables 3 and 4 for Cs and Pu, respectively). The rationale is that it is possible that the ultracentrifugation procedure was unable to remove the smallest colloids that had transported through the column, and thus there could have been some radionuclide mass in the supernatants that was assumed to be in solution but was actually associated with small colloids. Making this assumption increases the apparent desorption rate constant because the mass that was determined by ultracentrifugation to be in the solute phase in the injection solution had to be assumed to desorb from colloids in the column. The mass fraction is the same for the two sets of calculations because regardless of whether the radionuclides desorb from colloids in the column or outside the column (between injections), they must still be accounted for as desorbed mass.

The desorption rate constants at the upper end of cumulative probability distributions of Figure 19 are poorly constrained because any radionuclide mass that desorbed from the colloids during the first injection (or second injection for Pu) could have desorbed at a much more rapid rate than the rate deduced from fitting the radionuclide breakthrough curve. By fitting the data with a single rate constant, it is implicitly assumed that all the radionuclide mass had the same rate constant. In reality, any of the desorbed radionuclide mass could have desorbed at a higher rate than the fitted rate constant, and any of the non-desorbed radionuclide mass would have desorbed at a lower rate. The shaded regions at the upper right of Figure 19 indicate where the upper ends of the cumulative probability distributions could fall. A maximum desorption rate constant of 1 hr^{-1} was arbitrarily chosen for both Cs and Pu for the sake of illustration. The exact shape or upper limit of this end of the distributions was not interrogated by the column experiments, but these features are of little significance because the radionuclide mass fraction associated with this end of the distributions (i.e., shaded regions to the upper right) will desorb from the colloids almost immediately in a field setting (this fraction did not even transport through the columns).

Of much greater significance in Figure 19 is the lower end of cumulative probability distributions of desorption rate constants (lower left portion of plot). The black vertical dashed line in Figure 19 corresponds to approximately the lowest desorption rate constant that can be effectively distinguished from zero in the laboratory experiments. Any desorption rate constant to the left of this vertical line will result in negligible radionuclide desorption from colloids over the time scales of the column experiments. The location of this line is determined in part by the

inability to measure small deviations from 100% recovery for colloid-associated radionuclides because of the inherent scatter in the breakthrough curve data. If 99% recovery could be distinguished from 100% recovery, then the lowest measurable desorption rate constant would be about 0.0002 hr^{-1}. However, we consider the estimates of radionuclide recoveries to be accurate to within only about 5% or so given the data scatter, and 95% recovery translates to a desorption rate constant of about 0.001 hr^{-1}. The calculated Cs recovery in the third injection was close to 100%, but the fitting procedure yielded an estimate of 0.0009 hr^{-1}, which for all practical purposes is indistinguishable from a desorption rate constant of zero.

The shaded rectangular regions at the lower left of Figure 19 indicate where the lower ends of the cumulative probability distributions could fall. The colored dashed lines show potential extrapolations of the laboratory data trends to desorption rate constants that cannot be effectively interrogated in the experiments without significantly increasing column residence times (via either larger columns or lower flow rates or numerous additional injections). The true extrapolation of the cumulative probability distribution is critical for predicting colloid-facilitated transport over CAU time and distance scales. Using the lowest desorption rate constants that can be effectively measured in the laboratory column experiments, i.e., ~0.001 hr^{-1}, one would predict that 63% of the colloid-associated radionuclide mass would desorb after 1000 hrs of residence time in the system and over 99% would desorb after 10,000 hrs of residence time, or a little over a year. However, if a finite fraction of the colloid-associated radionuclide mass truly has a desorption rate constant of zero, or a value very close to zero, then colloid-facilitated transport over CAU time and distance scales would be possible. Thus, while the experiments conducted here cannot be used to unequivocally conclude that colloid-facilitated radionuclide transport will occur over CAU scales, the trends indicated by the column experiments certainly suggest that this is a possibility, particularly for Cs. We suspect that the same flattening of the lower end of the distribution of desorption rate constants observed for Cs would have been observed for Pu if another Pu injection could have been conducted.

A plot similar to Figure 19 could also be constructed for the colloid filtration rate constants, but since there was no apparent filtration after the first injection in each column, these plots would show that the majority of the colloid mass (80-90%) had a filtration rate constant of zero or near zero. We believe that the colloid filtration rate constants for the second and third injections were probably not truly zero, as indicated in Tables 3 and 4, but that they were simply too low to be distinguished from zero over the time scale of the experiments.

One of the potential criticisms of the repeat-injection methodology used in this study is that the re-injection of the recovered colloids and radionuclides into the same columns as previous injections could have led to misleading results because some of the colloid attachment sites and radionuclide sorption sites in the columns would have already been occupied during the second and third injections. While this is undoubtedly true, the masses of both colloids and radionuclides that were retained in the columns are very small relative to what would normally be considered to be a 'saturation' of sites, particularly in the case of the radionuclides. The radionuclide masses deposited in each column were approximately 2.3×10^{-5} g of Cs and 1.4×10^{-10} g of Pu, and if these masses were distributed evenly on the crushed tuff mass used to pack the columns, the mass loadings would be 5.9×10^{-8} g Cs/g tuff and 3.7×10^{-13} g Pu/g tuff. These loadings are much less than the expected adsorption capacities of the tuff. For instance,

assuming a partition coefficient of 10 ml/g, which is almost certainly too low for both Cs and Pu, the radionuclide concentrations in the first injection solutions would have been in equilibrium with 3×10^{-7} g Cs/g tuff and 9×10^{-12} g Pu/g tuff, respectively. Thus, the total adsorbed mass of both radionuclides after all injections was considerably less than what would have been in equilibrium with the first injection solution (even assuming a very small partition coefficient) which implies that the mass loading was much lower than the adsorption capacity of the tuff. Alternatively, if we assume a cation exchange capacity of 1 meq/kg for the tuff, which is over an order of magnitude less than the lowest Cs cation exchange capacity measured for six different volcanic tuffs from the Crater Flat unit near Yucca Mountain at the NNSS (Anghel et al., 2001), we calculate that the mass of Cs retained in the columns was over three orders of magnitude lower than the total cation exchange capacity of the columns. Given these calculations, it is difficult to make an argument that adsorption sites were exhausted in the experiments.

The possibility that deposited colloids may have occupied a significant fraction of the attachment sites in the column is not as easy to address. The deposited colloid mass in each column is estimated to be 5.7×10^{-5} g/g tuff and 2.1×10^{-5} g/g tuff, respectively, in the two columns, which are very low values. However, it is very difficult to predict how much surface 'blockage' is provided per unit mass of deposited colloids. Instead, we rely on multiple lines of indirect evidence to argue against a site 'saturation' effect that may have caused decreased filtration rates of the colloids with successive injections:

- The first Pu injection was conducted in the same column as the unspiked Chancellor water experiment, and despite the fact that the apparent attachment of colloids in the unspiked-water experiment was greater than in any other experiment, a significant fraction of colloids was still filtered in the first Pu injection.

- Colloid filtration for the first Cs injection appeared to be less than for the first Pu injection despite the fact that the Pu column had previously-deposited colloids and the Cs column did not. Also, the lack of apparent colloid filtration for the second Cs injection despite the significant filtration of colloids associated with the first Pu injection (which was a second injection into that column) strongly suggests that the observed filtration behavior was primarily a function of the colloid properties in the injection solutions, not the presence or absence of colloids already deposited in the columns.

- Colloid filtration observations and theory suggests a "ripening" effect that should increase colloid filtration as the mass of deposited colloids increases (e.g., Darby and Lawler, 1990), and this is the opposite of what was observed.

It is concluded that most likely explanation for the decreased filtration of colloids with each successive injection was that the columns effectively removed any colloids susceptible to filtration during the first pass through the column, and the remaining colloid population was inherently more resistant to filtration in subsequent injections.

Another potential criticism of the repeat-injection methodology is that retained colloid and radionuclide masses from previous injections could have exited the columns during subsequent injections, resulting in artificial higher recoveries of both colloids and radionuclides in the

subsequent injections. While we cannot unequivocally rule out the possibility of a partial contribution of previously-retained mass in each successive experiment, the background concentrations of colloids and radionuclides were allowed to drop to low levels before each successive injection, and the shapes of the breakthrough curves qualitatively suggest that the mass carryover between injections was minimal.

5. Conclusions

The conclusions of this study are:

1) The Chancellor water contains a relatively high colloid concentration of about 120 mg/L of colloids or about 2-3 x 10^{10} colloids/mL. The colloids are believed to consist mainly of clay and/or amorphous silicate materials. These colloids have a typical size distribution for NNSS cavity waters (most colloids less than 100 nm diameter), zeta potentials that are consistent with silicate/clay phases, and they appear to be very stable against aggregation or gravitational settling.

2) ^{137}Cs in the Chancellor water is approximately 50% partitioned to the colloids in the water, in good agreement with previous results (Reimus et al., 2006, Appendix C). The $^{239/240}$Pu partitioning to colloids in the unspiked Chancellor water was not measured in this study, but the partitioning after spiking the water with Pu(IV) nanocolloids was about 83%, and the partitioning after one column injection experiment was about 92%, which is nearly identical to the 90% partitioning in the unspiked water reported by Reimus et al. (2006) and Rose et al. (2011).

3) About 67% of the colloids and approximately 20% of the ^{137}Cs in the unspiked Chancellor water transported through the column packed with crushed Topopah Spring tuff. It is estimated that approximately 2/3^{rds} of the ^{137}Cs that was initially associated with colloids in the Chancellor water transported through the column on the colloids, and approximately 1/3rd of the colloid-associated ^{137}Cs desorbed from the colloids as a result of competitive sorption processes taking place in the column. There was no evidence that any solute ^{137}Cs exited the column, although the possibility of the transport of very small amounts of solute ^{137}Cs cannot be ruled out.

4) 85 to 95% of the colloids in the spiked Chancellor water experiments transported through the columns after the first injection, and the colloid recoveries after the second and third injections were indistinguishable from 100%. These results suggest that colloids susceptible to filtration were removed quite efficiently during the first injection, and the remaining colloids were highly resistant to filtration in subsequent injections. The difference between these colloid populations could not be attributed to size effects because there was no apparent difference in their size distributions.

5) The recovery of ^{137}Cs in the spiked Chancellor water column experiments steadily increased with each successive injection, starting at around 10% for the first injection, increasing to about 62% for the second injection, and rising to over 95% for the third injection. All of the ^{137}Cs transport through the column with each injection appeared to be associated with the

Chancellor colloids. The apparent desorption rate constants for desorption of ^{137}Cs from the colloids decreased by nearly two orders of magnitude from the first injection to the third injection, and in fact could essentially not be distinguished from zero for the third injection. These results clearly indicate that the ^{137}Cs that remained adsorbed to the colloids after each successive injection was more strongly associated with the colloids than in each previous injection.

6) The lower recovery of colloids but higher recovery of ^{137}Cs in the unspiked Chancellor water experiment relative to the first injection of the Cs-spiked Chancellor water is not fully understood. The colloid recovery was 67% for the unspiked water experiment and >90% for the spiked water injection, and the ^{137}Cs recovery was 20% for the unspiked water vs. 10% for the spiked water (or about 2/3^{rds} and 1/4th, respectively, of the ^{137}Cs adsorbed to the colloids in the injection solutions). We suspect that the colloid concentrations measured in the column effluent samples in the unspiked experiment may have been low because these samples were stored for several weeks before they were measured by the in-situ laser spectrometer, whereas the samples collected for the spiked water experiment were analyzed almost immediately. Also, the injected colloid concentrations in the unspiked water experiment may have been measured erroneously high, as the colloid concentrations exiting the column in both experiments were in reasonable agreement with each other, but the injection concentration in the unspiked experiment was reported to be about 30% higher than in the spiked experiment. The lower recovery of ^{137}Cs in the first injection of the Cs-spiked Chancellor water experiment may be attributable to the very large non-radioactive Cs spike in this experiment, which increased the overall Cs concentration in the water by nearly five orders of magnitude while increasing the ^{137}Cs concentration only slightly. Although this spike did not appear to affect the overall partitioning of ^{137}Cs to the colloids, it may have caused some of the ^{137}Cs originally associated with the Chancellor colloids to be displaced from stronger sorption sites on the colloids and thus be more susceptible to desorption during the first column injection.

7) The $^{239/240}$Pu recovery was relatively high for the first column injection of Pu-spiked Chancellor water, and then it decreased for the second injection, followed by an increase for the third injection. These results were obtained despite the fact that the measured $^{239/240}$Pu association with the Chancellor colloids increased with each successive injection. We suspect that the decrease in $^{239/240}$Pu recovery for the second injection can be attributed to the transformation of some of the Pu(IV) nanocolloids to either or both Pu(IV) and Pu(V) in solution, followed by re-partitioning of this dissolved material between the Chancellor colloids and the solution phase in the aftermath of the first injection. Despite the fact that the transformation of Pu resulted in greater partitioning of Pu to the colloids for the second injection (Table 4), the association of the Pu to the colloids was apparently somewhat weaker during the second injection than during the first injection, which led to a somewhat larger deduced desorption rate constant for the Pu from the colloids than for the first injection. The trend reversal in Pu recovery for the third injection is qualitatively consistent with the observed behavior in the spiked ^{137}Cs experiments in that the Pu appears to be more strongly associated with the colloids in the third injection than in the second injection.

8) The results of both the spiked ^{137}Cs and $^{239/240}Pu$ experiments suggest that there is a relatively rapid filtration of Chancellor colloids that are susceptible to filtration and a relatively rapid desorption of radionuclides from 'weaker' sorption sites on the Chancellor colloids, but as time and distance scales increase, mobile colloids are more likely to remain mobile and radionuclides adsorbed to colloids are more likely to remain adsorbed to the mobile colloids. In effect, there appear to be processes occurring that 'naturally select' for more mobile colloids and more strongly colloid-associated radionuclides as time and distance scales increase. These trends are consistent with field observations such as the transport of colloids and colloid-associated radionuclides originating from the Benham cavity on Pahute Mesa to locations significant distances downgradient, like ER-20-5 and ER-20-7 (Kersting et al., 1999; Zavarin, 2012).

6. References

Abdel-Fattah, A. I.., Zhou, D., Boukhalfa, H., Tarimala, S., Ware, S. D., and Keller, A. A. 2013. Dispersion Stability and Electrokinetic Properties of Intrinsic Plutonium Colloids: Implications for Subsurface Transport, *Env. Sci. Tech.*, 47, 5626-5634.

Anghel, I., H. J. Turin, and P. W. Reimus. 2002. Lithium Sorption to Yucca Mountain Tuffs, *Applied Geochemistry*, 17(6), 819-824.

Buddemeier R.W. and Hunt J.R. 1988. Transport of Colloidal Contaminants in Groundwater: Radionuclide Migration at the Nevada Test Site, *Appl Geochem*, 3:535–548.

Comans, R. N. J., J. J. Middelburg, J. Zonderhuis, J. R. W. Woittiez, G. J. De Lange, H. A. Das, C. H. Van Der Weijden. 1989. Mobilization of Radiocaesium in Pore Water in Lake Sediments, *Nature*, 367-369.

Darby, J. and Lawler, D. 1990. Ripening in Depth Filtration: Effect of Particle Size on Removal and Head Loss, *Env. Sci. Tech.*, 24, 1069-1079.

Drellack, S.L. and Prothro, L.B. 1997. Descriptive Narrative for the Hydrogeologic Model of Western and Central Pahute Mesa Corrective Action Units, Bechtel-Nevada, Las Vegas, NV.

Kersting, A.B. 2013. Plutonium Transport in the Environment, *Inorganic Chemistry*, 52(7), 3533-3546.

Kersting A. and Zavarin M. 2011. Colloid-facilitated transport of Pu at the NTS In: *Actinide Nanoparticle Research.* Ed. Kalymkov and Denecke, pp. 399-412, ISBN 978-3-642-11432-8.

Kersting A. B., Efurd D. W., Finnegan D. L., Rokop D. J., Smith D. K., and Thompson J. L. 1999. Migration of Plutonium in Groundwater at the Nevada Test Site. *Nature*, 397, 56-59.

Kersting, A. B. and P. W. Reimus, eds. 2003. "Colloid-Facilitated Transport of Low-Solubility Radionuclides: A Field, Experimental, and Modeling Investigation," *UCRL-ID-149688*, Lawrence Livermore National Laboratory, Livermore, CA.

Neck V, M Altmaier, A Seibert, JI Kim, JI Jun, CM Marquardt, and Th Fanghänel. 2007. Solubility and Redox Reactions of Pu(IV) Hydrous Oxide: Evidence for the Formation of PuO2+x (s, hyd), *Radiochimica Acta*, 93:193-207.

Reimus, P. W., M. Murrell, A. I. Abdel-Fattah, E. Garcia, D. Norman, S. Goldstein, A. Nunn, R. Gritzo, and B. Martinez. 2006. "Colloid characteristics and radionuclide associations with colloids in source-term waters at the Nevada Test Site (FY 2005 Progress Report)," *LA-UR-05-8612*, Los Alamos National Laboratory, Los Alamos, NM.

Reimus, P. W., G. Pohll, T. Mihevc, J. Chapman, L. Papelis, B. Lyles, S. Kosinski, R. Niswonger, and P. Sanders. 2003. "Testing and Parameterizing a Conceptual Model for Radionuclide

Transport in a Fractured Granite using Multiple Tracers in a Forced-Gradient Test", *Water Resources Research*, 39(12), 1350, doi:10.1029/2002WR001597.

Reimus, P. W. 2003. "Implications of Experimental Results/Interpretations and Previous Studies for CAU-Scale Colloid-Facilitated Radionuclide Transport," Chapter 11 in Kersting, A. B. and P. W. Reimus, eds. (2003) (see above).

Reimus, P. W., S. D. Ware, A. R. Humphrey, A. I. Adams, B. R. Wilson, D. Gonzales, R. G. Warren, and F. C. Benedict. 2002. "Diffusive and Advective Transport of ^{3}H, ^{14}C, and ^{99}Tc in Saturated, Fractured Volcanic Rocks from Pahute Mesa, Nevada," *LA-13891-MS*, Los Alamos National Laboratory, Los Alamos, NM.

Reimus, P. W. and M. J. Haga. 1999. "Analysis of Tracer Responses in the BULLION Forced-Gradient Experiment at Pahute Mesa, Nevada," *LA-13615-MS*, Los Alamos National Laboratory, Los Alamos, NM.

Rose, T. P., Hu, Q., Zhao, P., Conrado, C.L., Dickerson, R., Eaton, G.F., Kersting, A.B., Moran, J.E., Nimz, G., Powell, B.A., Ramon, E.C., Ryerson, F.J., Williams, R.W., Wooddy, P.T., and Zavarin, M. 2011. Radionuclide Partitioning in an Underground Nuclear Test Cavity. *UCRL-TR-409817*, Lawrence Livermore National Laboratory, Livermore, CA.

Tamura, T. 1972. Sorption Phenomena Significant in Radioactive-Waste Disposal, *Am. Assoc. Pet. Geol. Mem.*, 18:318-33.

Zavarin, M. 2012. "Isotopic Analyses: Environmental Monitoring Well ER-20-7", Memo to Bill Willborn, UGTA Sub-Project Manager, October 3, 2012, Lawrence Livermore National Laboratory, Livermore, CA.

Appendix A: Description of Volcanic Tuff Used in Column Transport Experiments

The following description is taken from Reimus et al. (2002). This description was based primarily on examination of a thin section made from a piece of intact core taken from borehole UE-20c, 2751 ft depth below surface (near the upper end of the 4-ft section of core that was used as the source of material for the column experiments). The description emphasizes fracture coating mineralogy, although it also includes a brief description of the matrix material. The description was provided by geologist F. Chris Benedict.

General Description

This material is described as devitrified moderately welded tuff from the Pahute Mesa lobe of the Topopah Spring Tuff of the Paintbrush Group (Tptm). This material comprises a welded tuff aquifer within the Topopah Spring Aquifer (Drellack and Prothro,1997). Multiple fractures are present in this sample. Two open fractures are exposed on the sample surface.

Optical Petrography

The polished thin section is a rectangular cut of core 12 by 20 mm that represents micro-granophyric moderately welded tuff with common pumice, mostly spherulitic and minor fine granophyric. Scarce to common felsic phenocrysts are mostly sanidine, lesser, moderately altered plagioclase, and rare small quartz. Alteration of plagioclase indicates some overprint of quartzofeldspathic alteration. Scarce voids with associated magnetite and ilmenite probably represent clinopyroxene pseudomorphs; biotite is also scarce. Lithics are scarce to rare. Both lengths of the polished section are discontinuously bounded by fractures (FR1 and FR2). An open fracture with an apparent maximum aperture of 0.12 mm is accompanied by a second open fracture (fracture 2) with an apparent maximum aperture of 0.087 mm. Petrographic examination indicates that these fractures are both partially coated with manganese oxides (PS). Both fractures have significant apparent porosity (60% void space).

Scanning Electron Microscopy (SEM)

The SEM used was a Tracor ADEM coupled with an EDS (energy dispersive spectrometry) system. Typical accelerator voltage used on the SEM varied from 10kV to 20kV. Portions (up to 5cm×5cm) of the natural exposed open fracture surfaces were separated from the main sample and carbon-coated for textural and mineralogical evaluation in the SEM.

SEM evaluation showed the fracture surface coating to be typically rough and granular although it is largely covered by a thin clay mat. Surface relief is minimal (on the order of 0.04 mm). Sixty to 70 percent of the fracture surface is coated with a thin “mat-like” covering comprised of approximately 90 percent smectite plus illite (based on EDS spectra) with small amounts of apatite, variable Fe oxides, and an unusual carbonate-rich aggregate that appears to be psuedomorphic. As shown in the back scattered electron image captured in Fig. A-1, this carbonate rich aggregate appears to have a hexagonal cross section. EDS spectra indicate the cation present in this carbonate to be predominantly cerium. Ce-carbonate is also locally

observed as overgrowths on apatite grains. A secondary electron image (Fig. A-2) showing the identical field of view as Fig. A-1 shows that the pseudomorph is not very distinct under secondary electrons. This indicates that the Ce-carbonate is at least partially covered by the clay.

X-Ray Diffraction (XRD)

A powdered subsample of the tuff was analyzed by XRD at LANL to obtain the bulk mineralogy of the sample. A Siemens D-500 powder diffractometer was used for the analysis, with a corundum (Al_2O_3) standard added to the sample (20% by wt) to allow quantification of mineral abundances. The XRD spectrum was analyzed using the FULLPAT procedure developed by Chipera and Bish (2002). The sample was found to consist of 44±2 wt% quartz, 53±7% feldspar, 1±1% mica, and 1±1% hematite.

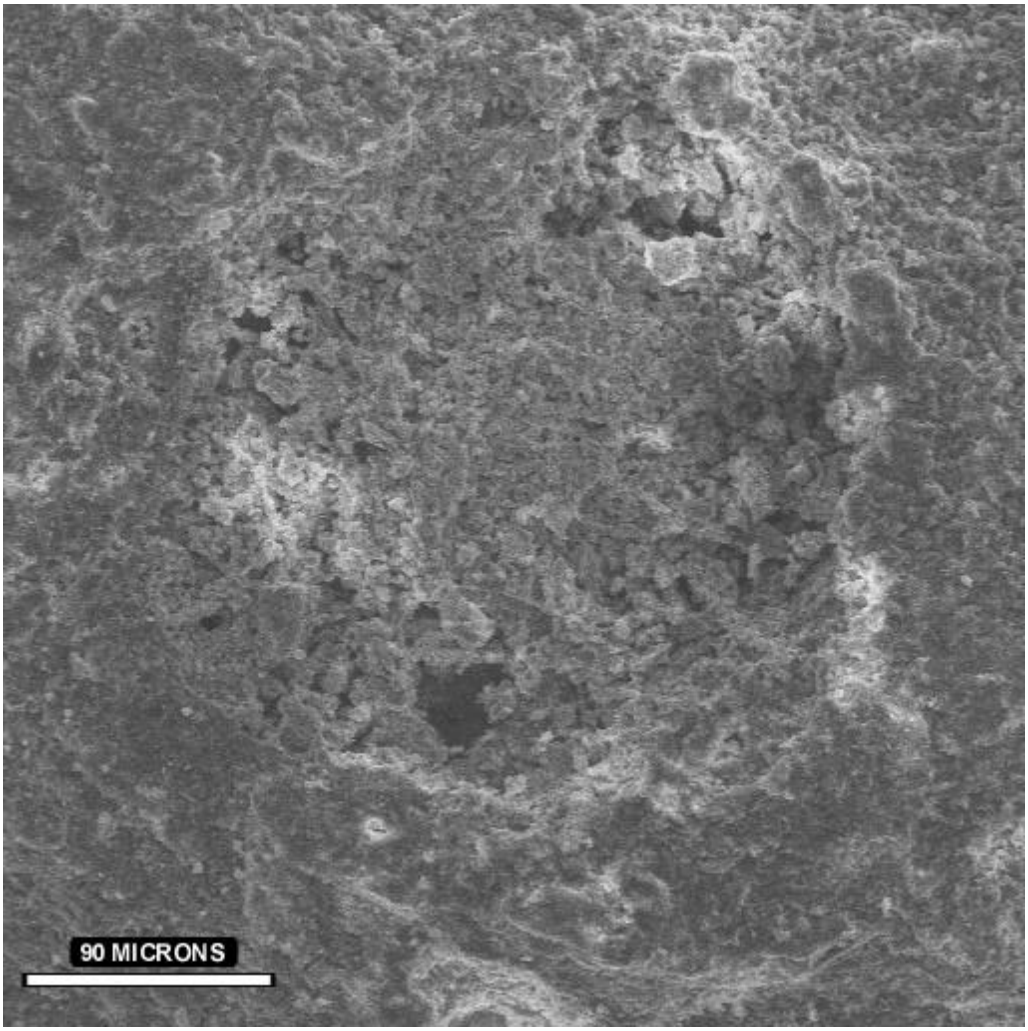

Figure A-1. Back scattered electron image showing pseudohexagonal outline of irregular aggregate of Ce-bearing carbonate (possible parisite/synchysite?).

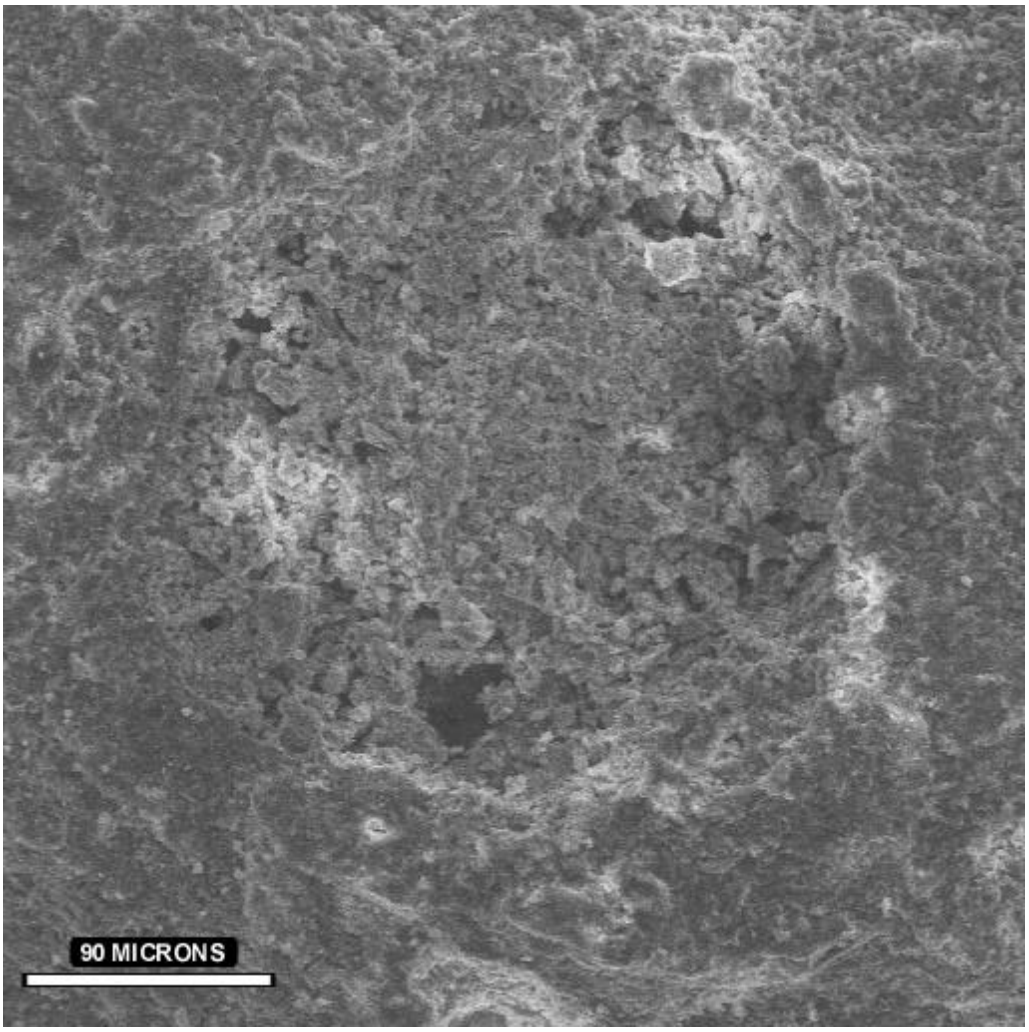

Figure A-2. Secondary electron image of the same field of view as in Figure A-1. Ce-carbonate aggregate is largely obscured by clay.